ANALYZING ANISOTROPY IN PERMEABILITY AND SKIN USING TEMPERATURE TRANSIENT ANALYSIS

A THESIS
SUBMITTED TO THE DEPARTMENT OF ENERGY
RESOURCES ENGINEERING
OF STANFORD UNIVERSITY
IN PARTIAL FULFILLMENT OF THE REQUIREMENTS
FOR THE DEGREE OF
MASTER OF SCIENCE

Kevin McCabe

June 2015

I certify that I have read this thesis and that, in my opinion, it is fully adequate in scope and quality as partial fulfillment of the degree of Master of Science in Petroleum Engineering.

(Roland Horne) Principal Adviser

Abstract

In many reservoir studies, anisotropic permeability values in orthogonal directions are often considered to have simple relationships. Often, this permeability anisotropy is modeled only between the vertical and horizontal directions as a certain ratio of values, while permeability values in a horizontal plane are considered equal. In reality, the depositional history of the reservoir results in more complex behavior. Knowledge of the permeability field has important implications in several different types of scenarios, thus it is important to have accurate estimates of these directional permeability values. A partially-penetrating well that allows for vertical flow to occur in the reservoir at depths below the bottom of the completed interval requires knowledge of vertical permeability anisotropy. In addition, improved estimates of horizontal permeability values would have significance for directional drilling purposes.

In this work, the utility of temperature data as a matching parameter was investigated to estimate these directional permeability values. The study utilized a full physics reservoir simulator and a nonlinear, least-squares regression algorithm for parameter estimation. By modeling block temperatures near the well that are output from the simulator, the study attempted to replicate the temperature data gathered from a Distributed Temperature Survey (DTS) which uses fibers to measure temperature history at the well. Using this method, the directional permeability values in the two scenarios described previously were estimated successfully with a high degree of accuracy. Additionally, the effects of a damaged zone surrounding the well in the horizontal case were investigated. In this case, the near-well, damaged zone permeability values were estimated successfully using temperature signals as well.

Acknowledgments

First and foremost, I would like to thank my advisor Prof. Roland Horne for his support, patience, and unmatched guidance. His role in my success has been instrumental and I will be forever grateful. I also thank the SUPRI-D consortium for the generous funding of this research, and the researchers of the group for their insightful advice and discussions.

I would also like to thank my friends and colleagues in the Energy Resources Engineering department for their assistance and support in classwork, research, and personal life.

Lastly, I would like to express my extreme gratitude towards my family. The love I've received from them for the duration of this work and beyond has kept me going through thick and thin, and I am very appreciative of their support.

Contents

List of Tables

List of Figures

Chapter 1

Introduction and Problem Statement

1.1 Background

Directional permeability values are often treated with simple relationships, despite the fact that the depositional history of the reservoir would result in complex heterogeneous and anisotropic behavior. Many studies model permeability anisotropy only between the vertical and horizontal directions as a predefined ratio (e.g. $k_v = 0.1 \times k_h$), while anisotropy between the permeability values in a horizontal plane is not modeled and the values are treated as equal (e.g. $k_x = k_y$). In well test analysis, pressure transients are analyzed to calculate a single permeability value, typically in tandem with the reservoir thickness such that the quantity kh is found. However, the assumption that a single permeability value can model flow behavior in all directions can cause errors in some calculations and contribute to the uncertainty of the problem. Knowledge of the permeability field as a whole has important implications in several different types of scenarios, thus accurate estimates of all directional permeability values is of importance. For example, a partially-penetrating well can have vertical flow

into the bottom of the completed interval, thus knowledge of the permeability in both the vertical and horizontal directions is required to determine the well performance. As another example, knowledge of the permeability values in the two orthogonal horizontal directions can improve decisions in directional drilling scenarios.

While the use of pressure transients have been used extensively for isotropic permeability calculations, their use to determine directional permeability values has been less common. Typically, estimation of directional permeability using pressure transient analysis would require measurements in multiple wells (see Ramey[11]). In this work, the use of temperature data from a single well to estimate these directional values was investigated. Schlumberger's Eclipse 300, a full physics thermal simulator, was applied to generate a forward model that output temperature data for analysis. By selecting block temperature outputs from the simulator, the method attempts to replicate the temperature data such as would be gathered from a Distributed Temperature Survey (DTS), which uses downhole fiber optic sensors to measure temperature history at the well. The temperature data were then used in a nonlinear, least-squares regression algorithm for parameter estimation. The least-squares difference between the forward model data and the updated models was minimized, with each iteration using updated parameters (directional permeability values) to drive the problem to the converged solution. A built-in Matlab function was used for this parameter estimation procedure.

Strongly coupled with the use of temperature transient analysis in this work is the assumption that the DTS completion strategy is capable of configuring the fibers in a specific setting. Specifically, when investigating horizontal permeability anisotropy, the completion of fibers in orthogonal directions surrounding the well is a significant factor in being able to estimate the directional permeability values. Although this

type of completion is unique in practice, several examples exist in the literature that describe the use of multiple fibers for downhole analysis (see Furniss et al. [5] and Koelman et al. [7]).

The existence of permeability anisotropy in the horizontal directions could also cause anisotropic skin effects in the near-wellbore region. Thus, the damaged zone surrounding the well and its effect on the temperature behavior was investigated as well. In this case, temperature data were used to estimate both the field permeability values in addition to the reduced, damaged zone permeability values. This scenario was also investigated using Eclipse 300, where a noncircular damaged zone was generated to simulate the anisotropic skin.

1.2 Prior Work

The measurement of permeability anisotropy has traditionally been investigated using specific types of wireline tools. Ayan et al. (1994) described several methods for estimating permeability anisotropy, including core analysis, wireline formation tests, and conventional well test analysis. Ehlig-Economides et al. (1990) also discussed the existence of permeability anisotropy in the context of optimizing production, and further described specific methods for measuring anisotropy.

While the use of temperature data for estimating permeability anisotropy may be a novel concept, many other studies have utilized temperature measurements in determining various formation properties and other production-related data. For example, Ouyang and Belanger (2006) provided a numerical approach to estimate flowrate profile from the distributed temperature profile. They found that DTS data could be

used to determine the production profile under specific circumstances, such as single-phase flow. Brown et al. (2005) also found that DTS data could be used to monitor production in a real developing field, providing another example of flowrate profiling from temperature measurements.

One of the more prevalent works for the progression of this study came from Sui et al. (2008), who developed a coupled wellbore and reservoir thermal model for parameter estimation in a multilayer formation. Using the Levenberg-Marquardt regression algorithm, temperature and pressure transient data were successfully inverted to estimate formation properties in multiple layers, including formation permeability, damaged zone permeability, and damaged zone radius. The basis for this study came from the work of Wang (2012), who provided a comprehensive investigation on the various uses of DTS data. It was found that temperature data could successfully estimate flowrate profile as well as formation properties in several different scenarios (e.g. multilayer formations, horizontal wells). Finally, the work of Mabunda (2014) showed that the thickness of the reservoir could be estimated successfully in constant-thickness models, and also provided a comprehensive sensitivity analysis on various thermal simulator parameters.

1.3 Report Organization

This report is organized as follows: Chapter 2 begins with a review of published methods that use temperature data for parameter estimation and other similar works. Chapter 3 details the methodology used in developing this work, including the simulator parameters and parameter estimation procedure used. Chapter 4 describes the two major scenarios of permeability anisotropy and their temperature effects. Chapter 5 contains the results from the various parameter estimation procedures and discusses

these results in further detail. Finally, Chapter 6 includes overall conclusions of this research and recommendations for future work on this problem and similar problems.

Chapter 2

Methodology

This chapter outlines the various properties input into the thermal simulator for the investigation, including grid and fluid properties in addition to well and timestep controls. Also included in this chapter is an explanation of the nonlinear, least-squares regression algorithm used to complete the parameter estimation of directional permeability values.

2.1 Simulator Parameters

2.1.1 Grid Construction

For this study, two different grids were constructed based on the two types of anisotropy investigation. Henceforth, the case that investigated permeability anisotropy between the vertical and horizontal directions (e.g. k_v and k_h) will be referred to as the "vertical anisotropy case" and the case that investigated permeability anisotropy with respect to the two orthogonal horizontal directions (e.g. k_x and k_y) will be referred to as the "horizontal anisotropy case" (see Figures 2.1 and 2.2).

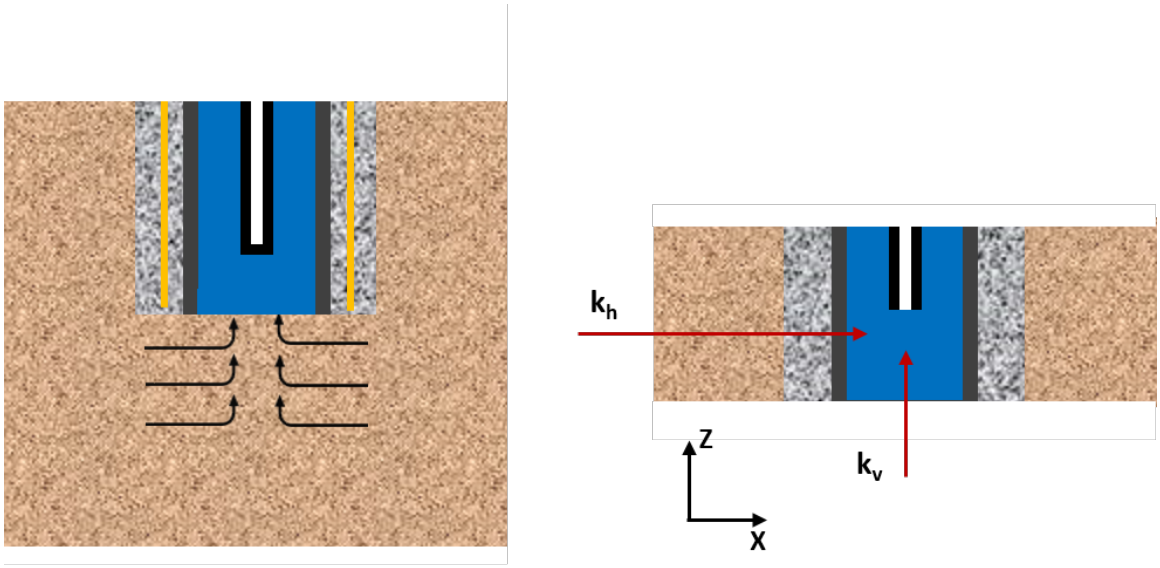

Figure 2.1: Reservoir diagram - vertical case

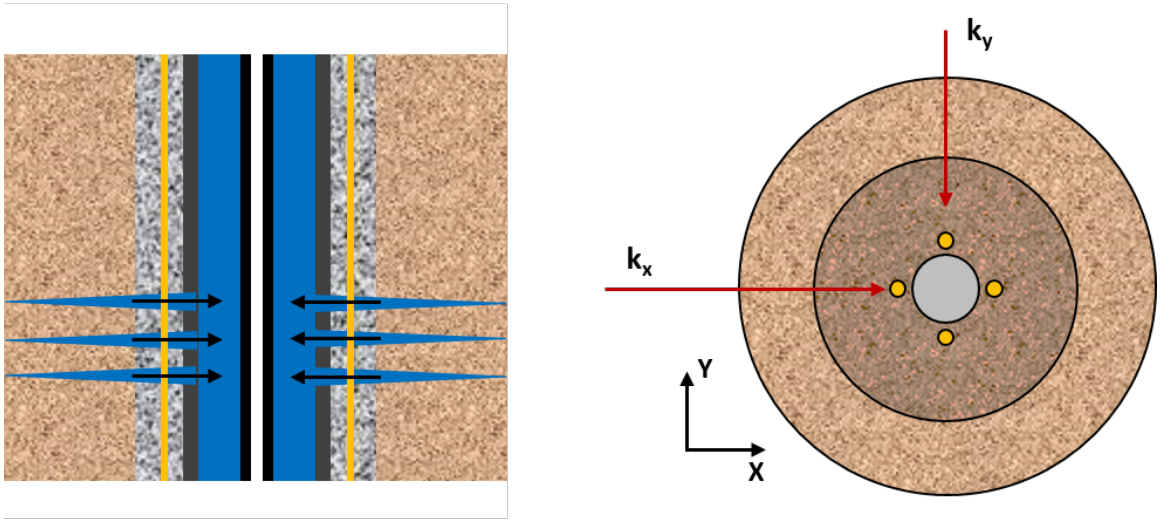

Figure 2.2: Reservoir diagram - horizontal case

For the vertical anisotropy case, a radial grid was constructed in order to model vertical and horizontal permeability anisotropy, where the horizontal permeability is represented by a radial permeability value (k_r) and is considered to represent equal values of k_x and k_y. In Eclipse, a radial model also requires a permeability value to be specified in the θ-direction, thus a constant value equal to the radial permeability was chosen. Table 2.1 gives more details on the dimensions and specific values used in the radial grid construction and Figure 2.3 shows the Eclipse visualization.

Table 2.1: Radial Grid Properties

Grid Type	Radial		
Dimensions	r 12	θ 1	z 30
Overburden Layers	1-5		
Reservoir Layers	6-25		
Underburden Layers	26-30		
Model Notes	Grid block size in r-direction increases monotonically and is a constant 10 ft. in z-direction.		

For the horizontal anisotropy case, a Cartesian grid was constructed in order to assign permeability values in the orthogonal horizontal directions, henceforth referred to as the "x" and "y" directions (see Figure 2.2). The permeability values in each direction varied with the type of test that was run, with anisotropy ratios between k_x and k_y ranging from two to ten. Table 2.2 gives more information about the grid properties and Figure 2.4 shows the Eclipse visualization.

Of particular importance in the horizontal anisotropy case is the completion of the DTS sensors around the circumference of the well. Specifically, the placement of *multiple* sensors around the well in orthogonal directions is significant in the horizontal case. The diagram on the right in Figure 2.2 gives a possible scenario where multiple

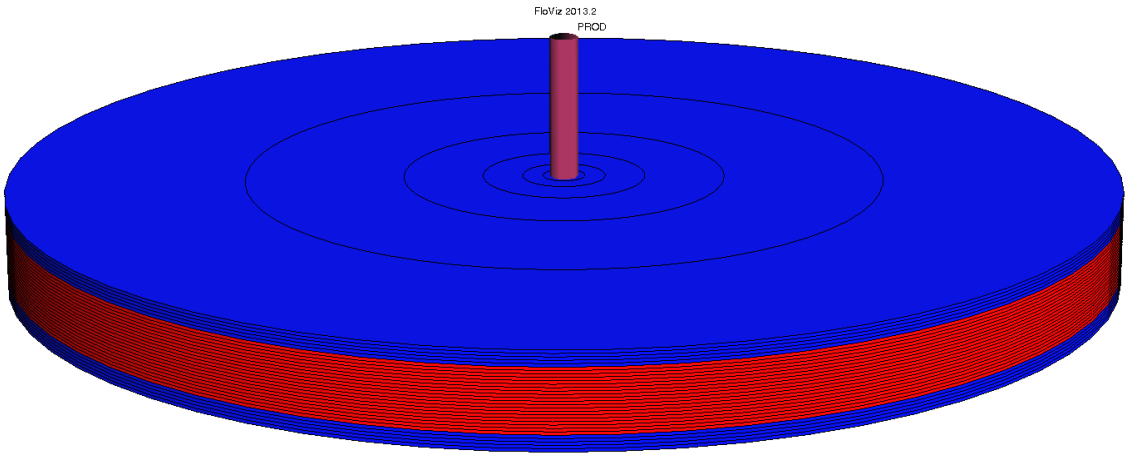

Figure 2.3: Radial grid - vertical anisotropy case

fibers in orthogonal directions are included in the completion. Such a completion in a real-world setting is unique, but ensuring that the correct placement could be achieved is necessary for the study of horizontal anisotropy. The assumption that the proper technology exists to ensure this placement had a significant role in the development of the analysis.

Several examples exist in the literature that describe multiple fiber completions. For example, Furniss et al. [5] described a configuration with two installed fibers for a coal seam gas project in Queensland, Australia. The fibers provided an early look into the behavior of the well, in addition to achieving subsurface allocation of well test kh. Another example is described in Koelman et al. [7], where, in a workshop-scale setting, multiple DTS fibers were run back and forth around the circumference of the well. This provided temperature measurements in each quadrant around the sand control system, ultimately providing insight into wellbore deformation as well as the mechanically and thermally induced strains on the system.

Table 2.2: Cartesian Grid Properties

Grid Type	Cartesian		
Dimensions	x 71	y 71	z 20
Overburden Layers	1-3		
Reservoir Layers	4-17		
Underburden Layers	18-20		
Model Notes	Grid block size in x and y increases monotonically away from well block. Size in z-direction is 10 ft.		

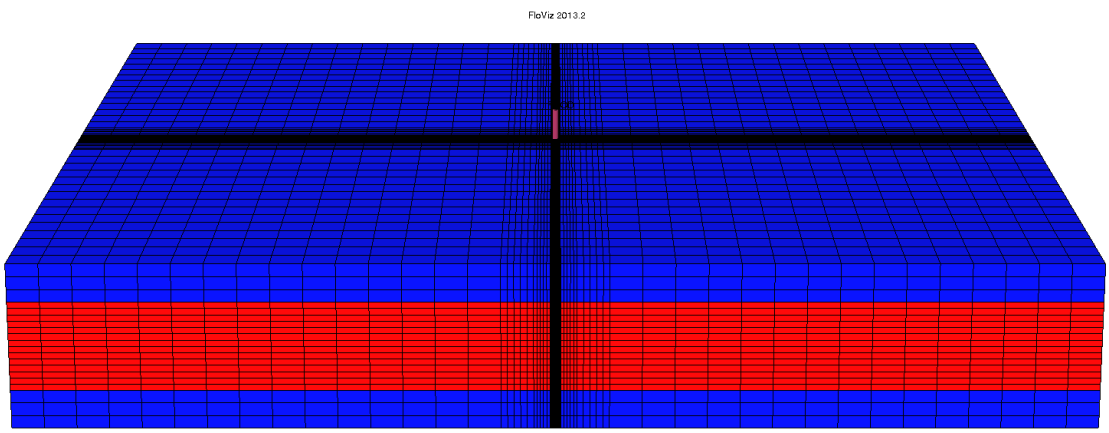

Figure 2.4: Cartesian grid - horizontal anisotropy case

In both cases, the reservoir is represented by a number of layers with a porosity of 23% and a nonzero permeability that was assigned based on the type of investigation. The remainder of the grid represented the overburden and underburden, and was modeled as layers having 0.1% porosity and zero permeability. As mentioned previously, directional permeability values differed depending on the case being investigated, but only this anisotropy was included and the permeability field as a whole was treated as otherwise homogeneous. All other rock-related properties, such as thermal conductivity and heat capacity, were also considered homogeneous.

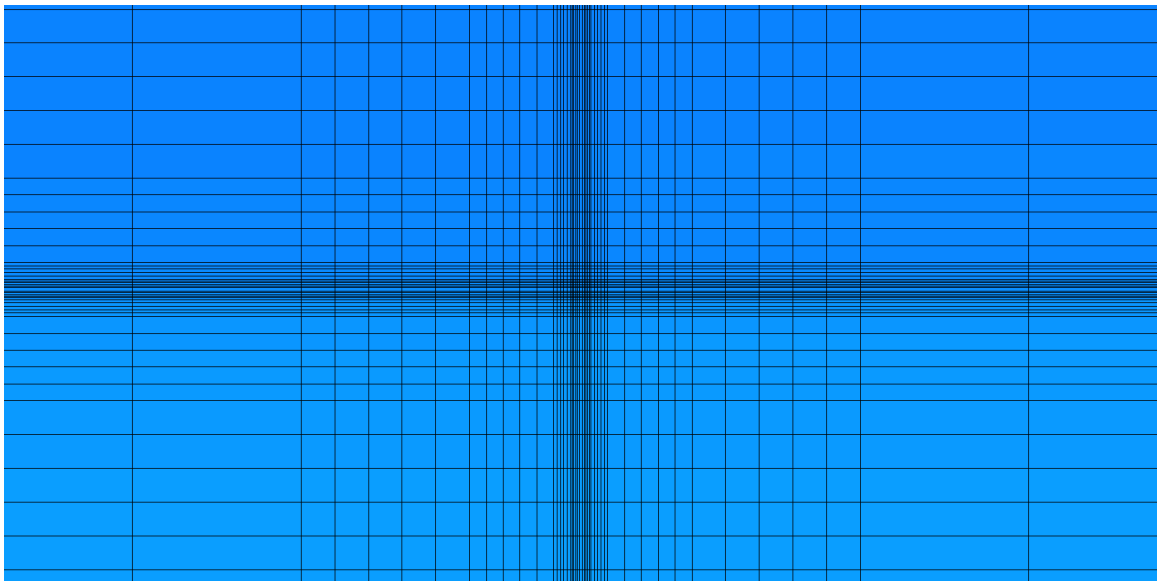

Figure 2.5: Visualization of grid refinement

The grid block sizes in both the vertical and horizontal anisotropy cases were not uniform, and increased monotonically from the central well block. In each case, the goal was to have a finely gridded model near the wellbore in order to better represent the temperatures that a DTS fiber would measure in a typical test. For example, in the horizontal anisotropy case, the grid block size near the boundaries of the reservoir was 50 feet and near the wellbore was 0.5 feet (see Figure 2.5). The temperature histories from the blocks surrounding the well block were then utilized in the subsequent analysis.

2.1.2 Fluid and Rock Properties

The reservoir models described in Section 2.1.1 were assumed to be homogeneous in petrophysical and fluid properties, despite being anisotropic in permeability. Several tests were completed with varying permeability anisotropy ratios, in order to better understand the limitations of the estimation method. Although these tests will be discussed in greater deal in a later section, some examples of the scenarios investigated

include large anisotropy ratios (e.g. $k_v/k_h = 10$), moderate ratios (e.g. $k_x/k_y = 5$), and small ratios (e.g. $k_x/k_y = 2$).

The porosity of the reservoir layers (modeling sandstone) was set to 23%, whereas the porosity in the overburden and underburden layers (modeling shale) was set to 0.1%. The thermal properties of the grid included those attributed to both rock and fluid (oil) and were considered to be constant and equal in both the "sand" and "shale". The rock heat capacity was set to 35 Btu/ft^3/°R and the thermal conductivity of both the rock and oil was set to 36 Btu/ft/day/°R. The oil for the single-phase investigation (i.e. $S_o = 1$) had a constant viscosity of 5 cp, density of 40 lbm/scf, specific heat of 0.15 Btu/lb/°R, and compressibility of 5×10^{-7} psi^{-1}. Finally, the initial reservoir pressure was set to 3500 psi and the initial temperature distribution was subject to a geothermal gradient of 15 °F/1000 ft, with the top layer set to 240 °F. Table 2.3 contains a summary of the essential rock and fluid properties used.

Table 2.3: Summary of Rock and Fluid Properties

Reservoir porosity	23	%
Initial reservoir pressure	3500	psi
Geothermal gradient	15	°F/1000 ft
Initial top layer temperature	240	°F
Rock heat capacity	35	Btu/ft^3/°R
Rock thermal conductivity	36	Btu/ft/day/°R
Oil saturation	100	%
Oil viscosity	5	cp
Oil density	40	lbm/scf
Oil specific heat	0.15	Btu/lb/°R
Oil thermal conductivity	36	Btu/ft/day/°R
Oil compressibility	5E-7	psi−1

Table 2.4: Well Placement Details

Model Type	Vertical Anisotropy	Horizontal Anisotropy
r-coordinate | x-coordinate	1	36
θ-coordinate | y-coordinate	1	36
Top vertical coordinate	6	4
Bottom vertical coordinate	15	17

2.1.3 Well and Timestep Controls

For both anisotropy cases investigated, only one well in production was used to obtain temperature data for the parameter estimation procedure. In the vertical anisotropy case (radial grid) the well was placed at the center of the grid and the blocks in the r-direction increased outward from that point. In the horizontal anisotropy case (Cartesian grid), the well was also placed in the center of the reservoir at block [36,36]. Consideration for the simulator's calculation of the well index parameter was given by ensuring that the size of the well block was large enough to accommodate the well diameter. In the Cartesian grid, this meant that the well block had a slightly large size than the surrounding blocks (e.g. 1 ft versus 0.5 ft).

The extent of the completed interval of the well was dependent on the type of investigation. In the vertical case, a partially-penetrated reservoir was the basis for the permeability anisotropy analysis, thus the completed interval only extends to 50% of the depth of the reservoir. This corresponded to layers 6 through 15 (recall that layers 6 through 25 constituted the full reservoir), or a penetration length of 50 ft into the reservoir. In the horizontal case, the reservoir was fully penetrated by the well from layer four to layer seventeen. This resulted in a full penetration length of 140 ft through the entire reservoir. Table 2.4 contains a summary of this information. Table 2.5 contains further information on the well controls used in the analysis.

Table 2.5: Well Control Details

Wellbore Diameter	0.3	ft
Oil Rate	1000	STB/day
BHP Constraint	50	psi
Control Scheme	Oil Rate	

Early analyses of temperature dependence on permeability anistropy showed that the early transient behavior was most significant for the parameter estimation procedure. Thus, the simulator was only run for a total of one day of production and the timesteps were selected to provide a sufficient number of data points for estimation. For the first 0.4 days the timestep used was 0.01 days, and the remaining 0.6 days used a timestep of 0.05 days. This timestepping scheme provided a total of 52 data points for temperature at each fiber location. In the horizontal case, the data from the two orthogonal blocks surrounding the well block were combined, thus the total number of points to be used in the estimation procedure was 104.

2.2 Parameter Estimation Procedure

The goal of this research was to investigate a parameter estimation procedure that used temperature history matching to estimate the permeability values in orthogonal directions. In a broader sense, this problem can be categorized as an optimization problem, where we attempt to minimize an objective function by varying the desired parameters. While a true application of this method would use temperature data from a real well in production, this study utilized the Eclipse 300 thermal simulator with the properties listed in the previous sections. The use of the simulator as a forward model provided temperature data for a proxy reservoir that attempts to replicate a real reservoir.

With regards to the two anisotropy cases investigated, there were two different approaches in gathering and preparing the temperature data for use in the algorithm. In both cases, a block temperature was output from the simulator (the "BTEMP" output in Eclipse) as opposed to the well temperature ("WTEMP"). This was to ensure that the temperature history utilized in the parameter estimation procedure was a function of the formation effects, and not a function of any effects that may occur in the well temperature calculation. In the vertical anisotropy case, the temperature history from the grid block at the bottom of the completed interval was used, to account for the temperature effects of vertical flow into the bottom of the interval. In the horizontal anisotropy case, block temperatures from two blocks were necessary for estimation of permeability in orthogonal directions. This required the output of temperature measurements from blocks that corresponded to the directional permeability values being estimated. Figure 2.6 shows the blocks used to obtain the temperature data. These were referred to informally as the "North" and "East" blocks for simplicity. In both cases, the selection of block temperatures was done to replicate the physical, real-world scenario of completing the well with DTS fibers installed. For the horizontal case, the successful estimation of directional permeability values would rely heavily on the appropriate placement of fibers in a real completion.

The procedure for the updating of parameters by use of a nonlinear, least-squares regression is described next. As mentioned previously, the forward model was created to replicate a real reservoir. The directional permeability values assigned to this model were treated as the true values that the procedure attempted to estimate. In each case, various types of anisotropy scenarios were tested. Three main scenarios were created for each case, a small, moderate, and large anisotropy ratio. Note that the anisotropy *scenarios*, which refer to the magnitude of the ratio of directional permeability values, are distinct from the anisotropy *cases*, which refer to the distinction

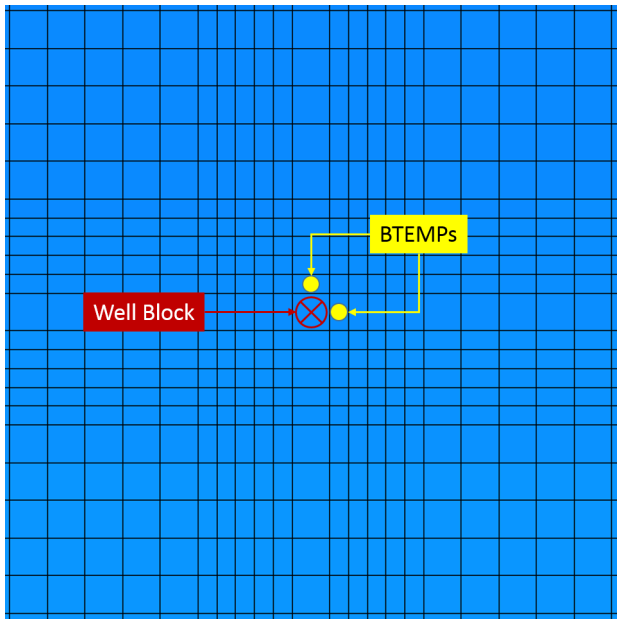

Figure 2.6: Block temperatures used in analysis

between vertical and horizontal anisotropy (see Figure 2.7). Table 2.6 contains the actual permeability values used in each scenario. These values were then written into an "include" file, an external file that can be updated and included into the appropriate section of the Eclipse input file. Once the simulation of the forward model was complete, the temperature data were extracted from the Eclipse output file and placed in a vector as input to the nonlinear regression. In the horizontal case, the temperature outputs for the North and East fibers were appended together to form a single vector.

To update the parameters (directional permeability values), a nonlinear, least-squares regression was used. In this research, the objective function was a least-squares difference between the actual temperature data (generated from the forward model) and the model temperature data (generated after each parameter update). The essential function of this method is to vary the specified parameters in order to match the temperature data from the updated model to the actual data, subject to a certain

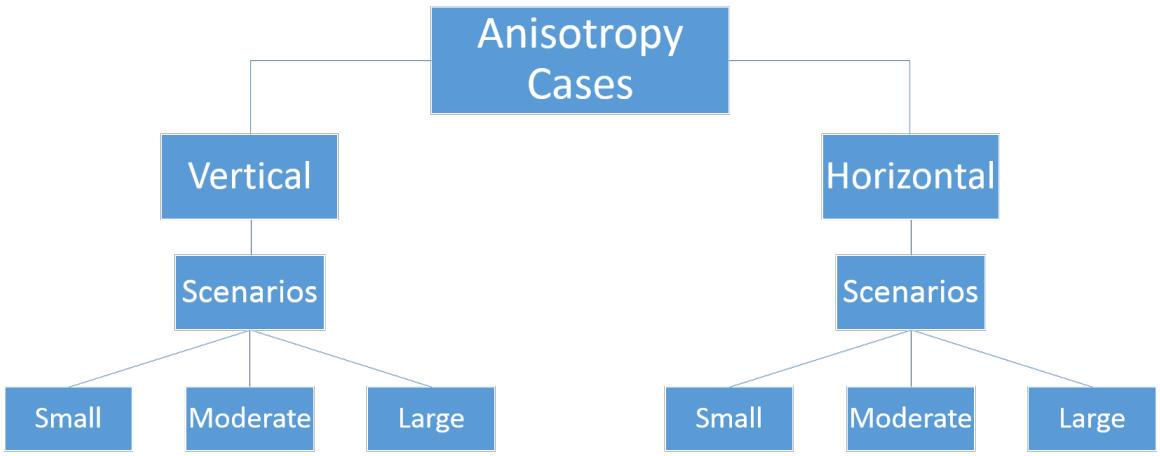

Figure 2.7: Organization chart showing hierarchy of study

convergence tolerance. In simple equation form, this is expressed as:

$$\sum_{i=1}^{N} \left(T_{actual_i} - T_{model_i}\right)^2 \tag{2.1}$$

where N is the total number of data points ($N = 52$ for the vertical case, $N = 104$ for the horizontal case).

The specific method used to update the parameters came from a built-in function from the Matlab Optimization Toolbox, named **lsqcurvefit**. Although the foundation of the method still relies on the least squares difference as a convergence criterion, the details of providing the function with the correct inputs was more complex. From the Matlab documentation[9] the full form of the function, which attempts to find coefficients x, is given as:

$$\min_x \|F\left(x, xdata\right) - ydata\|_2^2 = \min_x \sum_i \left(F\left(x, xdata_i\right) - ydata_i\right)^2 \tag{2.2}$$

where,

$$
\begin{aligned}
x &= \text{parameters to be updated (directional permeability values)} \\
xdata &= \text{input data (time)} \\
F(x, xdata) &= \text{function that returns temperature data from the inclusion of} \\
&\quad \text{parameters } x \\
ydata &= \text{observed output (forward model data)}
\end{aligned}
$$

For the purposes of this research, $F(x, xdata)$ was a function call to run Eclipse 300 with the parameters x, the directional permeability values. The function also required initial guesses for each parameter, which were treated as isotropic. The initial guesses for each anisotropy scenario are given in Table 2.6.

Table 2.6: Summary of Anisotropy Scenarios

	Vertical Anisotropy		**Horizontal Anisotropy**	
Permeability	k_v (md)	k_h (md)	k_x (md)	k_y (md)
Small Ratio	10	50	50	25
Moderate Ratio	5	50	50	10
Large Ratio	5	100	100	10
Initial Guess	25	25	20	20

The function **lsqcurvefit** has the ability to utilize one of two algorithms for parameter estimation: trust-region-reflective method and Levenberg-Marquardt method. The default option is the trust-region-reflective algorithm, which is a subspace trust-region method that is based on the interior-reflective Newton method. The basic idea of the algorithm is to approximate the objective function (sum of least-squares) with a simpler function that reasonably reflects the behavior of the original function in

a neighborhood around the previous iteration point. This neighborhood is labeled the trust region. The parameters are then updated within the simplified trust-region subproblem by calculating gradients and Jacobians by use of forward finite differences.

The use of **lsqcurvefit** required certain modifications for the specific application of the two scenarios that were analyzed for this research. The most significant change was the option titled "FinDiffRelStep", which used typical and observed values of parameters x to set the finite difference values. The default setting for this option caused finite difference steps that were too small for the Eclipse simulator to recognize. Recall that the parameters x represented the directional permeability values, thus finite difference steps on the order of 10^0 were ideal. Other modifications to the function included relaxed tolerances on the function value and x, however these changes were for simulation run-time limitations and did not affect convergence.

2.3 Summary

Two reservoir grids (see Figure 2.3 and Figure 2.4) were created to investigate two types of permeability anisotropy, dubbed "vertical anisotropy" (k_v and k_h) and "horizontal anisotropy" (k_x and k_y). Typical values of rock and fluid properties were applied for use in the Eclipse 300 thermal simulator, where the outputs of block temperature histories were used for analysis. For the vertical case, the block temperature at the bottom of the completed interval was used in order to capture the temperature effects due to vertical flow. For the horizontal case, block temperatures to the "North" and "East" of the well block were used in order to model multiple DTS fibers in orthogonal directions. A built-in Matlab function, **lsqcurvefit**, was prepared and utilized for a nonlinear, least-squares regression, which included parameter updating by use of a trust-region-reflective algorithm.

Chapter 3

Vertical Anisotropy

This chapter will focus on the vertical anisotropy case, previously described in Section 1.1. For this analysis, a partially-penetrating vertical well was considered and thus vertical flow into the bottom of the completed interval is possible. The chapter will be organized to include a more detailed description of the anisotropy case, as well as results from the parameter estimation procedure and discussion of the temperature behavior.

3.1 Case Description

The diagram that describes the vertical anisotropy case is reproduced in Figure 3.1. The subsurface scenario that led to such a configuration would include a well that partially penetrates the reservoir. The type of DTS completion is not as significant as in the horizontal anisotropy case, where the specific DTS fiber locations are necessary for the analysis. In the vertical case, a single fiber would be sufficient as long as the temperature measurement is taken at the bottom of the completed interval. This location allows for measurement of the temperature effects resulting from vertical flow from depths below the bottom of the completed interval.

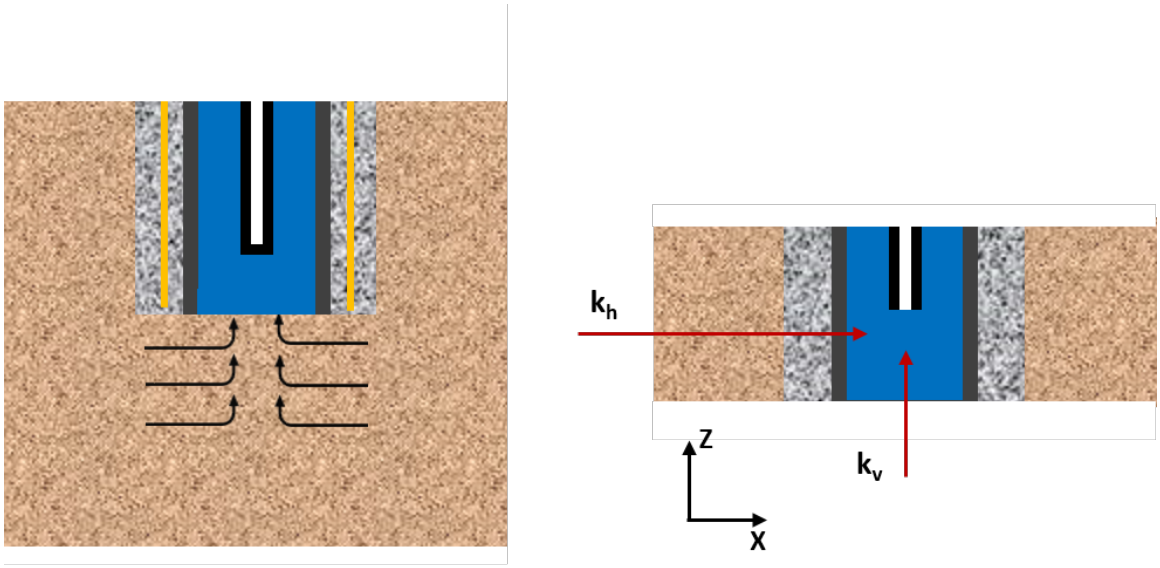

Figure 3.1: Reservoir diagram - vertical case

In the analysis, the temperature measurement is output from Eclipse as a block temperature (BTEMP) at the bottom of the completed interval. Thus, for the model described in Section 2.1.1, this would be the block temperature at the grid location $(r, \theta, z) = (1, 1, 15)$. Figure 3.2 helps to illustrate where this measurement is taken (note that the grid includes several extra radial slices for better visualization). Because the inner block of the radial model has a diameter of only 0.5 ft, the use of the block temperature output at this location should be representative of the effects a DTS fiber would measure. The discrepancy between vertical and horizontal flow regimes near the bottom of the completed interval could be quantified by a fiber at any location around the wellbore, thus the block temperature replicates the scenario sufficiently well.

Although the methodology and use of the thermal simulator was discussed in Section 2.1, some additional details relating only to the vertical anisotropy case are

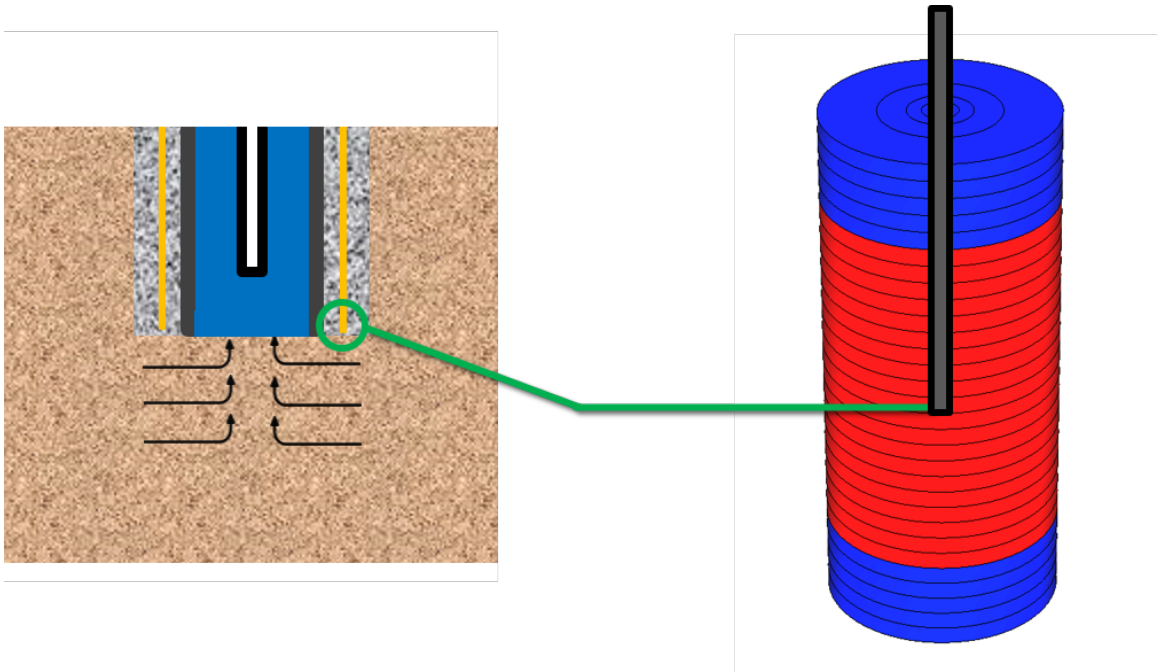

Figure 3.2: Temperature measurement location

provided here. Of particular importance was the choice of a radial model for investigating vertical anisotropy. For this case, the assumption was made that the radial permeability value, k_r, would be representative of a general "horizontal" permeability, k_h. Because the value of radial permeability was kept as a constant for this case, this allowed for the investigation of a purely vertical anisotropy, which analyzed the directional permeability values in the vertical and horizontal directions explicitly. To extend this idea further, the horizontal permeability described the permeability values in the x- and y-directions, such that only one permeability value given for k_h would represent isotropic permeability between k_x and k_y. The advantage of such an approach (the use of a radial grid) was that it allowed for greater efficiency in the nonlinear regression. Each simulation run was significantly shorter than for a Cartesian grid, allowing for more anisotropy scenarios to be investigated.

In order to better understand the relationship between vertical anisotropy and temperature behavior, many different scenarios were created to test the parameter estimation procedure. However for the purposes of this report, only three scenarios and their regression results are reported. The scenarios included here are titled "small", "moderate", and "large", in an attempt to describe the nature of the anisotropy *ratio* between the vertical and horizontal permeability (k_v/k_h). The summary showing the permeability values for each scenario is reproduced in Table 3.1. Of note in this table is the inclusion of an "Initial Guess" entry. These entries correspond to the permeability values used as the required initial guess for the nonlinear regression function. Although it is often assumed in reservoir studies that the permeability in the vertical direction is a proportion or fraction of the horizontal permeability (e.g. $k_v = 0.1 \times k_h$), an initial guess assuming isotropic permeability was used instead. This was a further attempt to test the robustness of the parameter estimation procedure.

Table 3.1: Summary of Vertical Anisotropy Scenarios

	Vertical Anisotropy	
Permeability	k_v (md)	k_h (md)
Small Ratio	10	50
Moderate Ratio	5	50
Large Ratio	5	100
Initial Guess	25	25

Additional tests of robustness included the introduction of synthetic noise to the forward model temperature data before applying the nonlinear regression procedure, which will be discussed in the next section.

3.2 Results and Discussion

The results portion of this vertical anisotropy analysis refers primarily to the regression results, namely the types of permeability values that were output from the parameter estimation procedure. However, strongly coupled to these results are various examples of temperature behavior that demonstrate the relationship between vertical anisotropy and the corresponding temperature measurements. Thus, this section will report the results of the vertical anisotropy scenarios described previously, then continue with discussion of these results in the context of the corresponding temperature behavior.

3.2.1 Regression Results

The nonlinear regression algorithm that was used to estimate the directional permeability values (k_v and k_h) proved to be very effective in all three scenarios and many more. As mentioned previously, only three types of scenarios are reported here, but are meant to be representative of the abilities of the both the algorithm to estimate directional permeability values, as well as the research findings in general. While other scenarios were tested during this investigation, the three reported here represent a range of anisotropy ratios between vertical and horizontal permeability.

Table 3.2 includes a summary of each of the investigated scenarios and the regression results. Note that the relative error is calculated as:

$$RelativeError = \frac{|y_{true} - y|}{y_{true}} \tag{3.1}$$

where,

$$y_{true} = \text{true values}$$

$$y = \text{regression results}$$

As the table shows, the results from the nonlinear regression had a high degree of accuracy, correctly estimating the directional permeability values with a maximum relative error of only 1.4% (in the large ratio scenario).

Table 3.2: Vertical Anisotropy Regression Results

	Small		**Moderate**		**Large**	
	k_v (md)	k_h (md)	k_v (md)	k_h (md)	k_v (md)	k_h (md)
True Value	10	50	5	50	5	100
Initial Guess	25	25	25	25	25	25
Results	10.1	50.0	5.00	50.0	5.07	100.0
Relative Error	1%	0.1%	0%	0%	1.4%	0.1%

In an attempt to replicate the type of temperature measurements taken from a real test with a DTS completion, another regression analysis was performed with the inclusion of synthetic noise to the temperature signal. Due to the unavailability of real temperature data, the addition of this noise was an attempt to investigate any limitations of the method, especially the ability of the nonlinear regression to converge to the correct solution when the data are noisy.

To accomplish this regression analysis, Gaussian noise was added to the original temperature data. The noise added to the signal was selected randomly from the normal distribution, then scaled by the maximum observed value as well as an additional scaling parameter ($\epsilon = 0.001$). The final result represents noise taken from

a normal distribution with standard deviation equal to the maximum temperature measurement, such that the original signal is masked by the addition of the noise. The additional scaling factor was introduced to dampen the raw noise. Equation 3.2 shows the details of the calculation of the noise, printed using Matlab syntax.

$$T_{noisy} = T + n_1 \tag{3.2}$$

$$n_1 = \epsilon \times \sigma \times \text{randn}(1, N) \tag{3.3}$$

where,

$T =$ unaltered temperature data from forward model

$\epsilon = 0.001 =$ scaling factor

$\sigma = \max_i |T_i| =$ standard deviation

$\text{randn}(1, N) =$ N-length vector of samples from normal distribution

$N =$ total number of data points

Figure 3.3, Figure 3.4, and Figure 3.5 show the temperature histories at the measurement block (i.e. DTS fiber location) for each scenario. The altered temperature signal is shown in red, and the noisy measurements that constitute these datasets were used as inputs to the nonlinear regression algorithm. Note that, while the dependent (temperature) scale is different for each plot, the change in magnitude (ΔT) is the same in each.

The results from the use of the noisy temperature signal in place of the original, forward model signal in the parameter estimation procedure are summarized in Table 3.3. Clearly the addition of noise to the signal introduced more error to the regression results. In general, the estimation of the horizontal permeability values

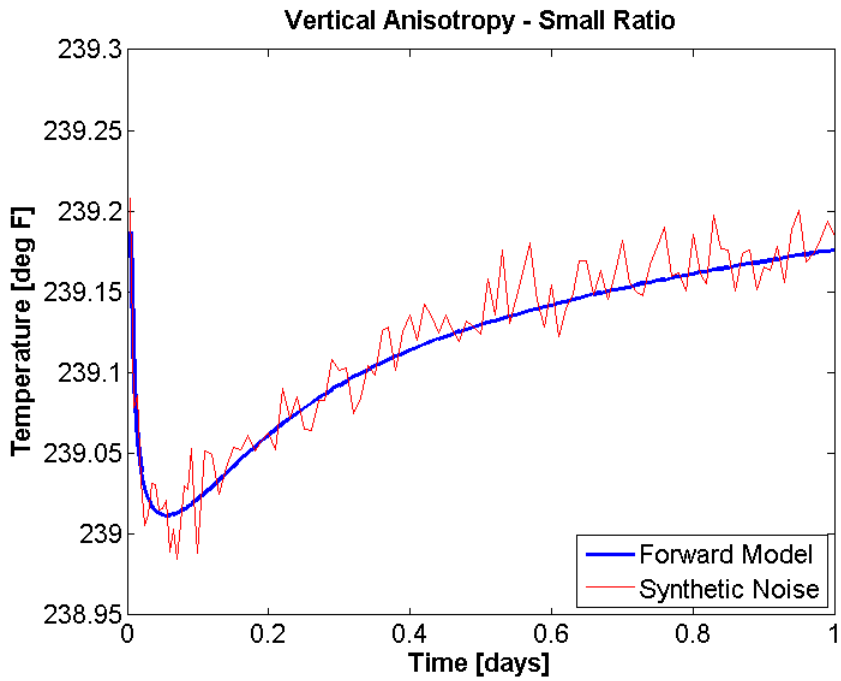

Figure 3.3: Temperature history with noise - small ratio

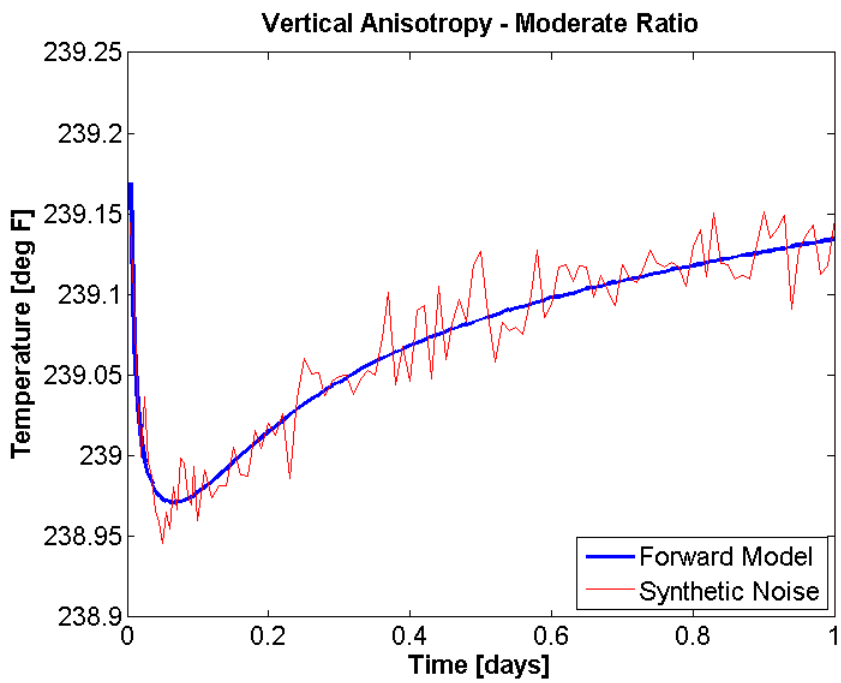

Figure 3.4: Temperature history with noise - moderate ratio

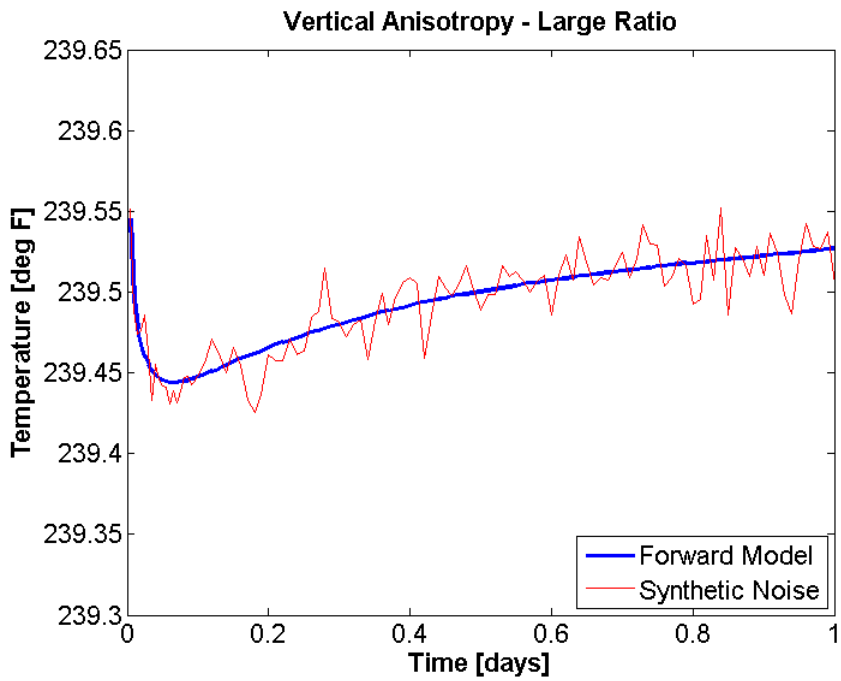

Figure 3.5: Temperature history with noise - small ratio

(k_h) was more accurate than that of the vertical values (k_v), and the large ratio scenario had rather large errors in both values. Although the relative error for k_v in the small ratio case appears to be large, it should be noted that the absolute error was only 3.7 md, thus the relative error result should be minded accordingly.

The large errors for the large ratio scenario may be explained by examining the plot of the temperature history in Figure 3.5. The original temperature signal (blue line) shows that a maximum temperature change of only about 0.1 °F occurs over the duration of the test. While this temperature history was used successfully to estimate the directional permeability values in the original regression, the small change in temperature verges on being not sufficient or unique enough for either accurate DTS measurement or for use in the nonlinear regression algorithm. With the addition of noise to the original dataset, the signal becomes convoluted and the nonlinear

Table 3.3: Vertical Anisotropy Regression Results - Noise Added

	Small		**Moderate**		**Large**	
	k_v (md)	k_h (md)	k_v (md)	k_h (md)	k_v (md)	k_h (md)
True Value	10	50	5	50	5	100
Initial Guess	25	25	25	25	25	25
Results	13.7	48.7	4.68	50.2	82.2	80.2
Relative Error	36.7%	2.6%	6.5%	0.3%	>100%	19.8%

regression could not converge on a unique solution.

3.2.2 Discussion of Temperature Behavior

The temperature behavior that is associated with vertical anisotropy is discussed next. Because the configuration of the vertical case included a partially-penetrating well, it should be expected that the vertical distribution of temperature shows a more distinct signature of anisotropy. This would demonstrate the discrepancy between two different types of flow regimes, the horizontal (radial) flow into the well, as well as any vertical flow that may occur at depths beneath the completed interval. Two different visualizations of the spatial temperature distribution are shown here, including the radial distribution and vertical distribution. Also included is a presentation of the temporal distribution of the temperature behavior at the location of the block representing the DTS fiber.

The radial distribution of the temperature signal does not show behavior that is unique to a scenario where vertical anisotropy exists, however several figures are shown to orient the reader to the progression of the test and the accompanying temperature changes. Figure 3.6 shows the progression from early time to 0.5 days, half the length of the total test. The initial temperature of the reservoir was approximately

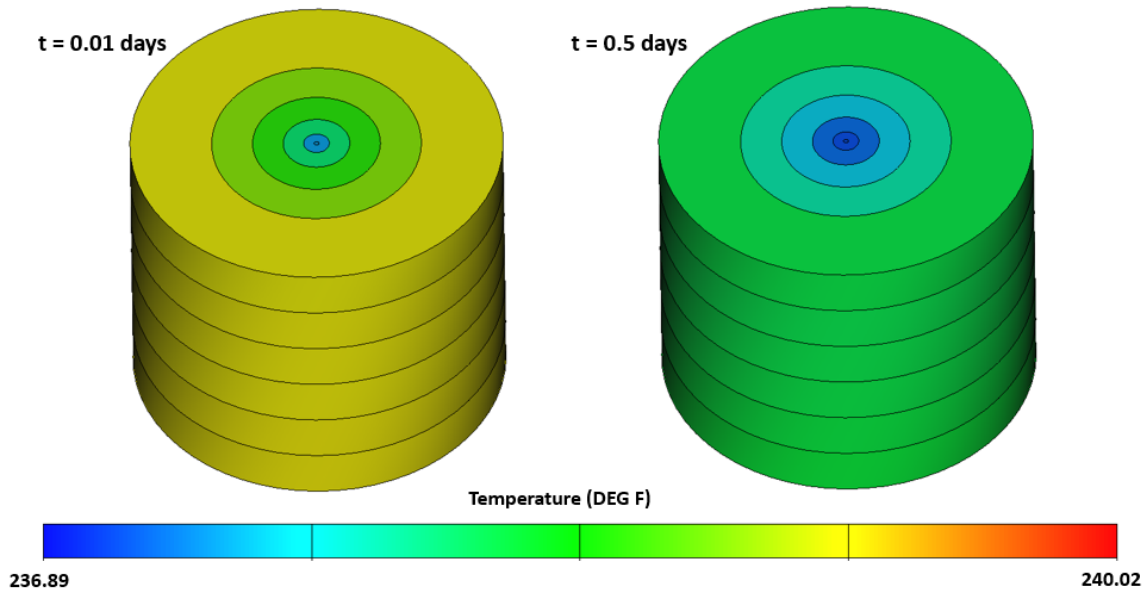

Figure 3.6: Radial distribution of temperature

240 °F, thus there was a quick change in temperature after just the first timestep. As the test progressed, the temperature trend was decreasing and the diagram on the right side of the figure shows a clear decrease in temperature after 0.5 days.

While the radial temperature distribution does not show any particular behavior that demonstrates the existence of vertical anisotropy, the vertical distribution near the wellbore in fact does. As mentioned previously, the premise for this vertical anisotropy investigation included a partially-penetrated well completion, and thus also included the potential for vertical flow into the bottom of the completed interval. Therefore, a distinct temperature signal should be seen in the area of the bottom of the completion. Figure 3.7 gives a visualization of the early time temperature behavior for each anisotropy ratio examined.

There is a clear distinction of temperature behavior between the zone of the completed

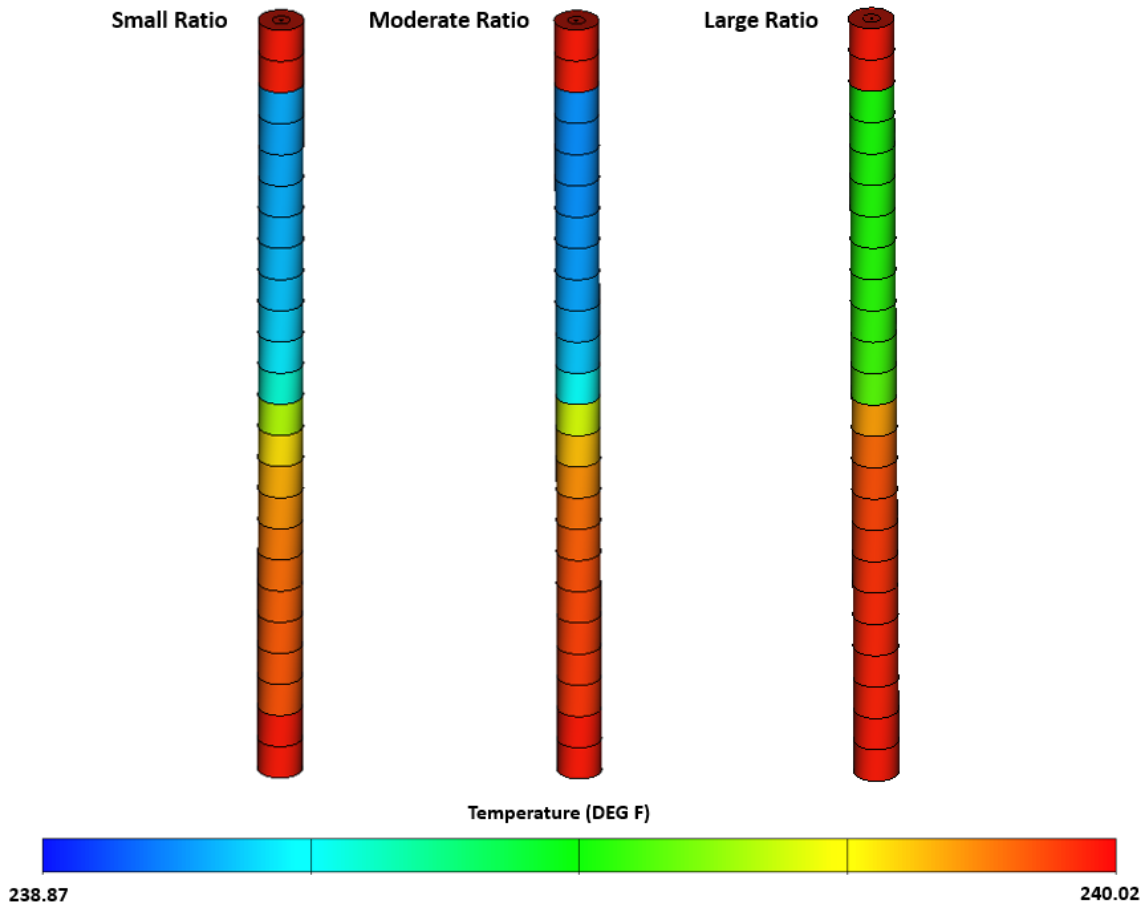

Figure 3.7: Vertical distribution of temperature

interval (denoted by lower temperature values) and the zone below the completed interval (higher temperature values). It appears that the vertical flow regime has drastically different effects on the temperature signature below the depths of the completed interval. We can deduce that any vertical flow through the reservoir into the well is relatively small compared to the radial flow into the well, due to the smaller vertical permeability and the presence of spherical rather than radial flow. There is a distinction between the different anisotropy scenarios, demonstrating a clear relationship between vertical anisotropy and temperature behavior.

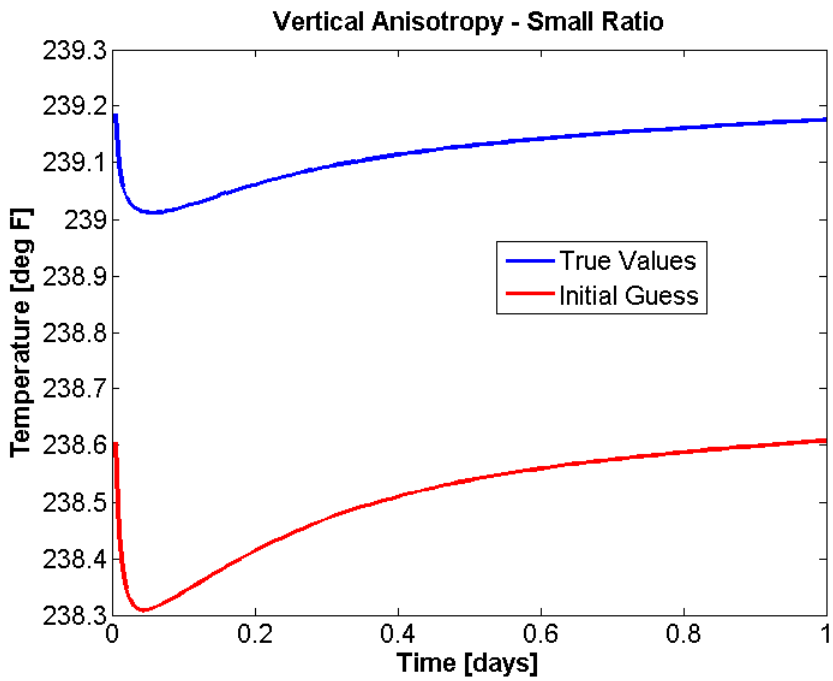

Figure 3.8: Temperature history - small ratio

Lastly, the temporal history of the temperature measurements for each scenario enhances the understanding of the relationship between temperature behavior and vertical anisotropy. Figure 3.8, Figure 3.9, and Figure 3.10 show the temperature history plots for the small ratio scenario, moderate ratio scenario, and large ratio scenario, respectively. Each plot also contains the temperature history attributed to the isotropic initial guess given to the nonlinear regression algorithm (see Table 3.1).

The distinctions between each scenario include slight perturbations in the shape of the plots, however more relevant is the magnitude of temperature change from the minimum to maximum measured values over the duration of the test. Recalling the discussion of the vertical temperature distribution, the contribution of vertical flow appeared to be very small in each scenario. Thus, the temperature measured at the block/fiber has a correspondingly small change in temperature throughout the test.

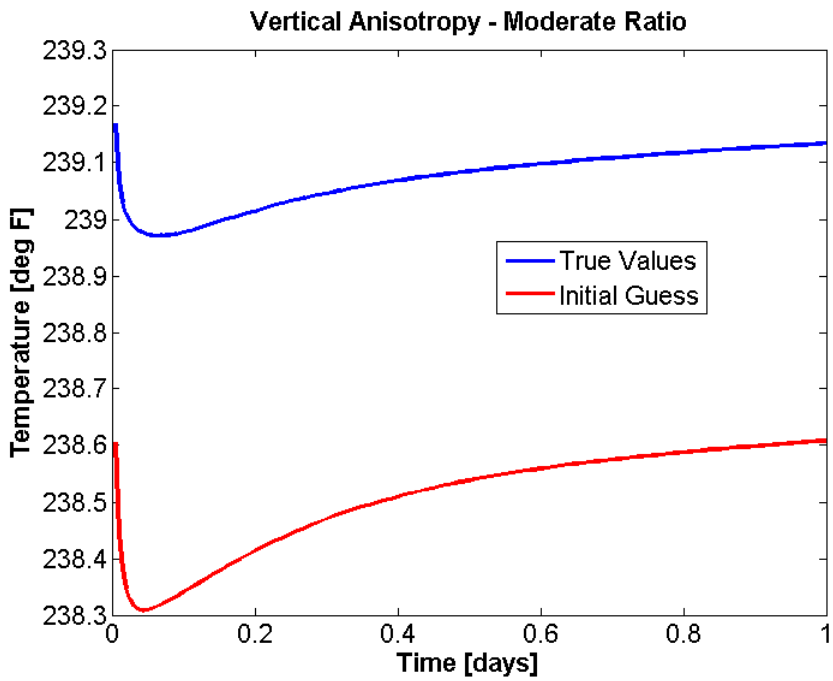

Figure 3.9: Temperature history - moderate ratio

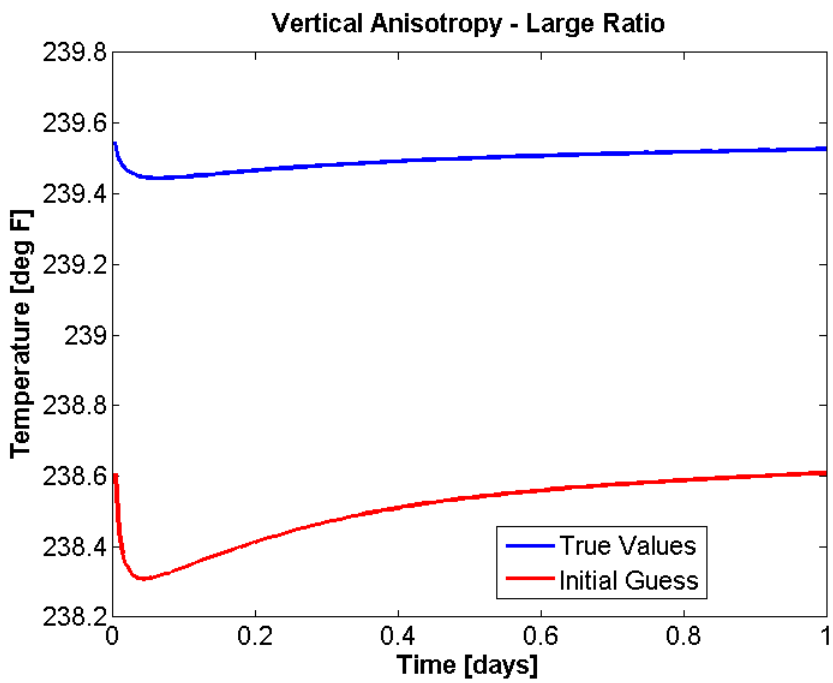

Figure 3.10: Temperature history - large ratio

The magnitude of this change is about 0.2 °F in the small and moderate scenarios, but only about 0.1 °F in the large scenario. It appears that the large difference between the vertical and horizontal flow regimes at the measurement block serves to reduce the effect of any vertical flow into the bottom of the interval, thus resulting in a small temperature change over the duration of the test. Nonetheless, these magnitudes of temperature change are measurable, and matching the history of the change did in fact allow the permeability anisotropy to be estimated correctly.

3.3 Summary

The investigation of this vertical anisotropy case was originally meant to be an initial analysis of the relationship between permeability anisotropy and temperature behavior. The analysis of the vertical case proved to be very successful and in many ways confirmed the potential usage of temperature transient analysis for parameter estimation purposes; specifically, for the estimation of anisotropy effects. This chapter showed that in three distinct scenarios of vertical permeability anisotropy, represented by small, moderate, and large anisotropy ratios (k_v/k_h), the nonlinear regression algorithm was quite successful in estimating the directional permeability values. The addition of synthetic noise as an attempt to replicate real DTS data also had some success in estimating the correct parameters. Furthermore, the temperature signatures of the vertical anisotropy case were shown, demonstrating a relationship between the temperature measurements in a partially-penetrating well completion and the existence of vertical anisotropy.

Chapter 4

Horizontal Anisotropy

This chapter will focus on the horizontal anisotropy case, previously described in Section 1.1. For this analysis, a vertical well that fully penetrates the formation was considered. Horizontal (radial) flow into the completed interval and the associated temperature transient behavior was investigated under the assumption of a specific type of DTS fiber completion, which will be explained in more detail in this chapter as well. Also included are the results from the parameter estimation procedure and further discussion of the temperature behavior. Finally, the chapter concludes with a brief discussion of the temperature behavior associated with anisotropy in skin.

4.1 Case Description

The diagram that describes the horizontal anisotropy case is reproduced in Figure 4.1. The subsurface configuration that was considered for such an investigation included a vertical well that fully penetrated the formation, with a completed interval that spanned the thickness of the reservoir. Thus, for this anisotropy case, the effect

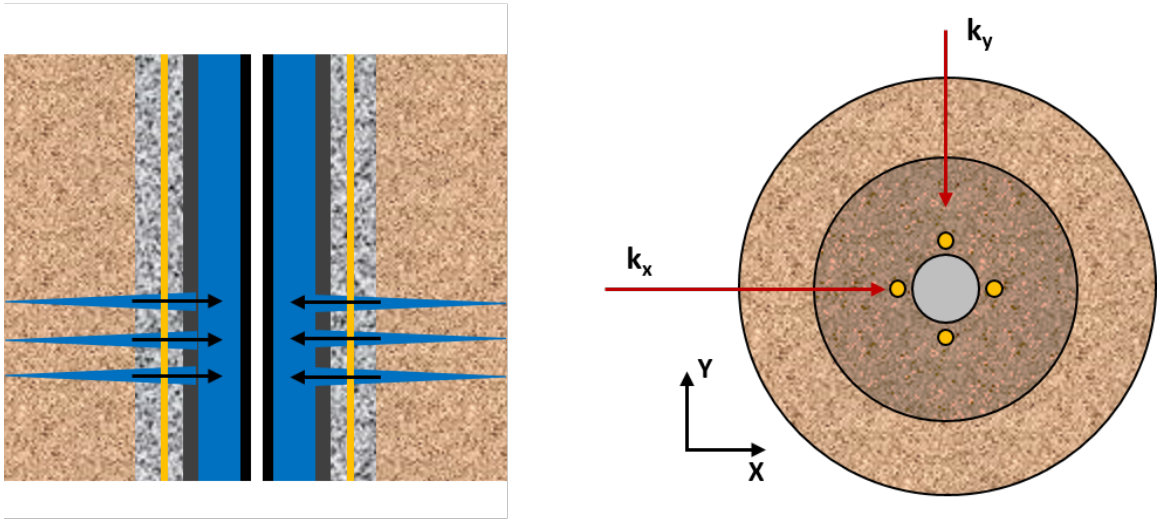

Figure 4.1: Reservoir diagram - horizontal case

of solely horizontal (radial) flow on the temperature transient signature was analyzed. While only a fully-penetrating well was considered for this case, a partially-penetrating well could also be investigated, provided the temperature measurements were taken at a depth in which any effects of vertical flow would not interfere with the temperature signal. Unlike the vertical anisotropy case, the type of DTS completion and, specifically, the location of the multiple fibers surrounding the well becomes more sensitive in the horizontal anisotropy case. Section 2.1.1 discussed such a completion, and the successful results of the nonlinear regression proved to be extremely dependent on the correct locations of the fibers in this study.

Similar to the vertical anisotropy case, in order to model the type of completion necessary for the horizontal anisotropy analysis, specific block temperature (BTEMP) outputs were taken from Eclipse and used as forward model temperature data. As mentioned previously, a Cartesian grid was used to accomplish this. Because this case analyzed temperature effects due to anisotropic permeability, and thus anisotropic

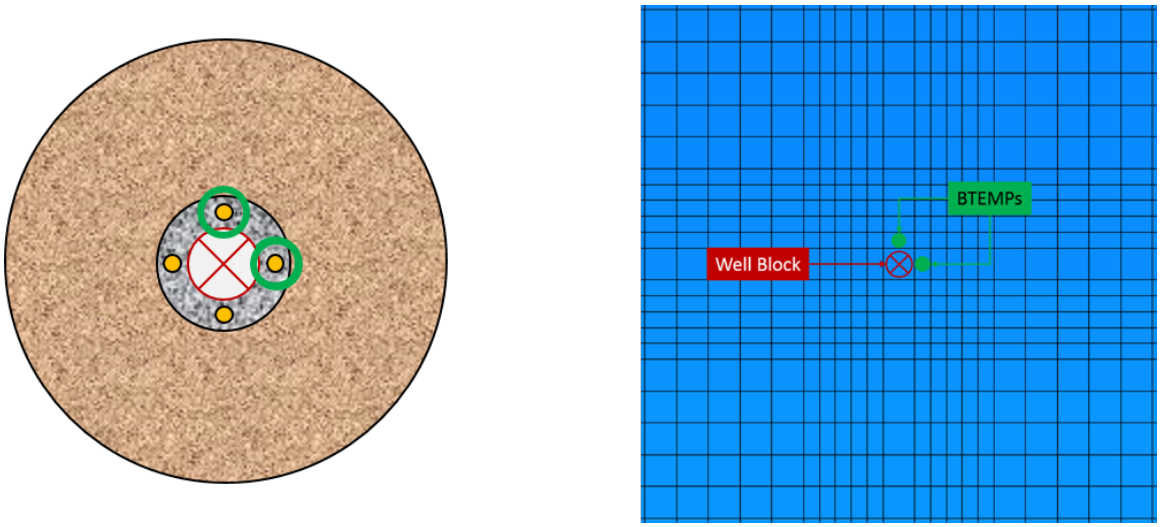

Figure 4.2: Temperature measurement locations for horizontal anisotropy case

flow, two distinct temperature measurements were necessary for the parameter estimation procedure. These measurement locations were in orthogonal directions and taken from the grid blocks directly neighboring the well block in the Cartesian grid. This setup replicated the multiple DTS completion necessary for this case; because the grid was refined near the well, the neighboring blocks were a distance of only 0.5 feet from the well block. This ensured that the temperature signal at these locations was representative of the measurements a real fiber might take. Figure 4.2 helps to illustrate where these measurements were taken. The two blocks used in the analysis were at grid locations $(x, y, z) = (36, 35, 11)$ and $(x, y, z) = (37, 36, 11)$ which were referred to as the "North" and "East" fibers, respectively. Note that, due to the symmetric nature of the reservoir, any combination of orthogonal grid block temperatures could be used (e.g. North-West or South-East).

As in the vertical case, there were other details specific to the horizontal anisotropy case that were not addressed in the overview discussion of the thermal simulator in Section 2.1. Of particular importance was the use of a Cartesian grid instead of the

radial grid used in the analysis of vertical anisotropy. This change was necessary due to the distinction of flow in the two orthogonal horizontal directions, the x- and y-directions, resulting from anisotropy in permeability. The Cartesian grid allowed for the necessary block temperatures to be output from the simulator, in addition to having the ability to assign directional permeability values correctly (e.g. k_x and k_y). It should be noted that, although the permeability field was anisotropic, the reservoir was considered to be otherwise homogeneous, thus every grid block was assigned the same permeability value for each directional permeability value.

Another distinction from the vertical case was the depth of the temperature measurements utilized in the horizontal anisotropy investigation. While the correct depth (i.e. the correct block temperature in the z-direction) was necessary in the vertical case to capture the effects of vertical flow into the completed interval, the depth at which the measurements were taken was less sensitive in the horizontal case. This was due to the fact that the configuration was a fully-penetrating well in the horizontal case. Thus, the temperature measurements at any depth within the completed interval could be used in the nonlinear regression, with the only difference being the initial reservoir temperature due to the geothermal gradient. As mentioned previously, the depth at which the measurements were taken for this analysis was near the center of the reservoir at block $z = 11$ (note that $z_{top} = 4$, $z_{bottom} = 17$).

In the absence of vertical flow drawing up warmer fluid from below, the trend associated with the vertical anisotropy case was found to be different from that of the horizontal anisotropy case. Chapter 3 included plots of the temperature history for the various anisotropy scenarios investigated, where each showed an initial sharp decrease in temperature followed by an increase for the remainder of the test. The

results presented in this chapter on horizontal anisotropy will include plots of the temperature history that show a decreasing temperature trend for the duration of the test.

In order to better understand the relationship between horizontal anisotropy, temperature transient behavior, and the corresponding regression results, several different anisotropy scenarios were created and tested. However, the same three types of scenarios used in the vertical anisotropy investigation will also be used in this chapter to illustrate the investigation of horizontal anisotropy. The scenarios, again titled "small", "moderate", and "large", describe the nature of the anisotropy *ratio* between the two orthogonal horizontal permeability values (k_x/k_y). It should be noted, however, that the actual values of the various ratios differ from those in the vertical case. The summary showing the permeability values for each anisotropy scenario is reproduced in Table 4.1. Of note in this table is the inclusion of an "Initial Guess" entry, which corresponds to the permeability values used as the required initial guess for the nonlinear regression function. Because isotropic permeability values in the x- and y-directions are often assumed in reservoir studies ($k_x = k_y$), the initial guesses for each anisotropy scenario were isotropic as well. This was an attempt to understand the relationship between the anisotropy ratios and the robustness of the parameter estimation procedure, in addition to providing a look into the ability of the procedure to depart from the normally assumed isotropic values.

Finally, much like the vertical anisotropy case, the use of constant simulator parameters and similar reservoir models in the horizontal case led to a questioning of the solution uniqueness for each anisotropy scenario. To investigate this concern, synthetic noise was introduced to the forward model temperature data for each scenario before applying the nonlinear regression procedure. The results of this analysis, including plots of the additional noisy data, are included in the following section.

Table 4.1: Summary of Horizontal Anisotropy Scenarios

	Horizontal Anisotropy	
Permeability	k_x (md)	k_y (md)
Small Ratio	50	25
Moderate Ratio	50	10
Large Ratio	100	10
Initial Guess	20	20

4.2 Results and Discussion

This section describes the regression results of both the unaltered and noisy scenarios, which includes the permeability values that were output from the parameter estimation procedure. However, this section will also examine the various types of temperature behavior in order to analyze the relationship between horizontal anisotropy and the corresponding temperature measurements. Thus, this section will report the results of the horizontal anisotropy scenarios described previously, then continue with discussion of these results in the context of the corresponding temperature behavior. Finally, the analysis will be extended to include a similar look at the effects of anisotropy in skin on the temperature signatures. This will include results from the nonlinear regression, where both field permeability and damaged zone permeability values were estimated, as well as a similar discussion of the temperature behavior associated with the presence of anisotropic skin.

4.2.1 Regression Results

The nonlinear regression algorithm that was used to estimate the directional permeability values (k_x and k_y) again proved to be very effective in all three scenarios described previously and many others not included in this report. It is assumed for the horizontal anisotropy case as well that the results for the three scenarios reported here are representative of the abilities of the parameter estimation procedure to estimate the directional permeability values as well as the research findings in general. Despite the fact that other scenarios were tested during this investigation, these three should represent a sufficient range of anisotropy ratios between the two horizontal permeability values.

Table 4.2 includes a summary of each of the investigated scenarios and the regression results. Once again, the relative error reported in the table is calculated as:

$$RelativeError = \frac{|y_{true} - y|}{y_{true}} \tag{4.1}$$

where,

$$y_{true} = \text{true values}$$
$$y = \text{regression results}$$

The table shows that the results from the nonlinear regression had a high degree of accuracy and correctly estimated the directional permeability values with a maximum relative error of only 0.2% in the large ratio scenario.

Because the specific type of DTS completion needed for this investigation is considered rather novel and not yet widely used in practice, there was no real temperature

Table 4.2: Horizontal Anisotropy Regression Results

	Small		**Moderate**		**Large**	
	k_x (md)	k_y (md)	k_x (md)	k_y (md)	k_x (md)	k_y (md)
True Value	50	25	50	10	100	10
Initial Guess	20	20	20	20	20	20
Results	50.0	25.0	50.0	10.0	100.2	9.98
Relative Error	0%	0%	0%	0%	0.2%	0.2%

data available to test the method. Thus, in an attempt to replicate the type of temperature measurements taken from a test with such a DTS completion, an additional regression analysis was completed with the inclusion of synthetic noise to the temperature signal output from the thermal simulator. The addition of this noise, as in the vertical anisotropy case, allowed for a further investigation into the robustness of the method, in particular the abilities of the nonlinear regression to converge to the correct solution when the data are noisy.

The procedure for adding the synthetic noise to the temperature data output from the simulator is the same as that used in the vertical anisotropy case. Gaussian noise was added to the signal by random selection from the normal distribution, then scaled by the maximum observed value of the temperature data as well as an additional scaling parameter ($\epsilon = 0.0005$). The final results represents noise taken from a normal distribution with standard deviation equal to the maximum temperature measurement, such that the original signal is masked by the addition of this noise. The additional scaling factor was introduced to dampen the raw noise, and ensure that the data was consistent with DTS measurement capabilities (e.g. data resolution). Equation 4.2

shows the details of the calculation of the noise, printed using Matlab syntax.

$$T_{noisy} = T + n_1 \tag{4.2}$$

$$n_1 = \epsilon \times \sigma \times \text{randn}(1, N) \tag{4.3}$$

where,

$T =$ unaltered temperature data from forward model

$\epsilon = 0.0005 =$ scaling factor

$\sigma = \max_i |T_i| =$ standard deviation

$\text{randn}(1, N) =$ N-length vector of samples from normal distribution

$N =$ total number of data points

Figure 4.3, Figure 4.4, and Figure 4.5 show the temperature histories at the location of the fibers (block temperatures) at the North and East blocks neighboring the well block. The noisy temperature signal is shown in red for each fiber measurement. The measurements that constitute these noisy datasets were then used as inputs to the nonlinear regression algorithm.

The results from the use of the noisy temperature signal in the parameter estimation procedure are summarized in Table 4.3. The addition of noise to the signal introduced a small amount of relative error in each scenario as compared to the analysis with no noise. Despite this, the regression was very successful in interpreting the signals with noise, and the absolute errors were no more than 2 md from the true values in all scenarios. Of particular note are the results from the large scenario case, which had the lowest amount of relative error of all scenarios and only a small increase in error from the analysis with no noise.

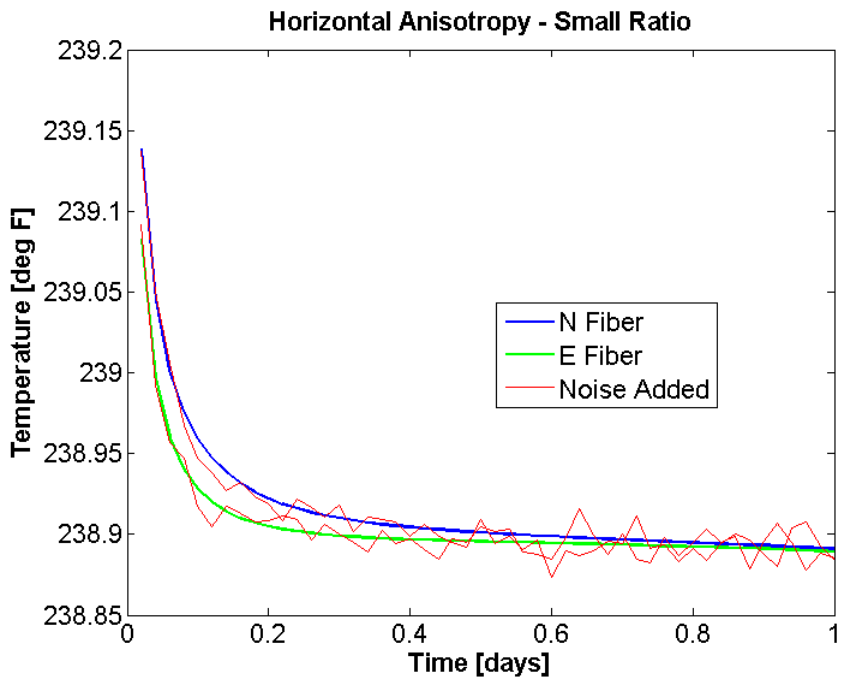

Figure 4.3: Temperature history with noise - small ratio

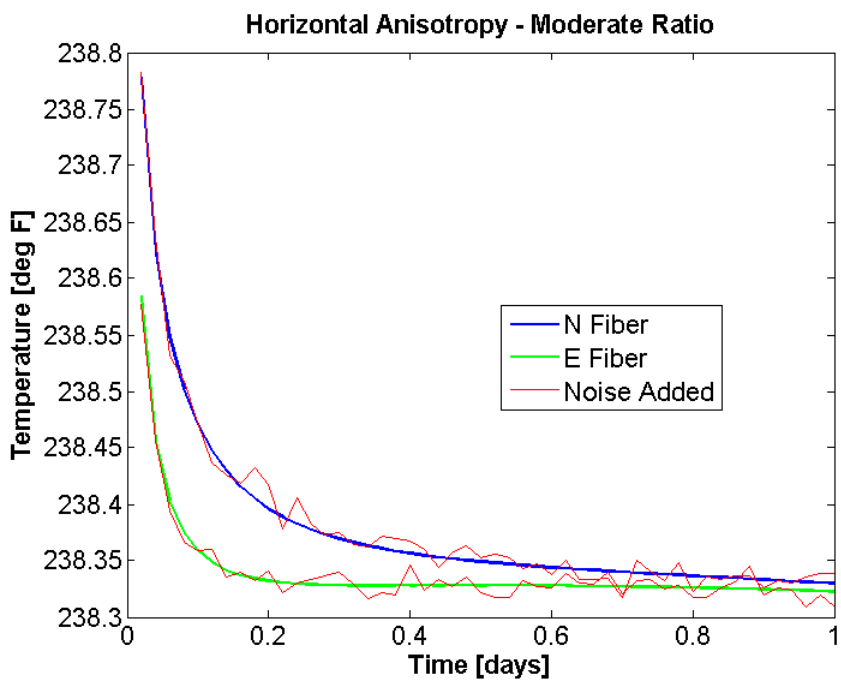

Figure 4.4: Temperature history with noise - moderate ratio

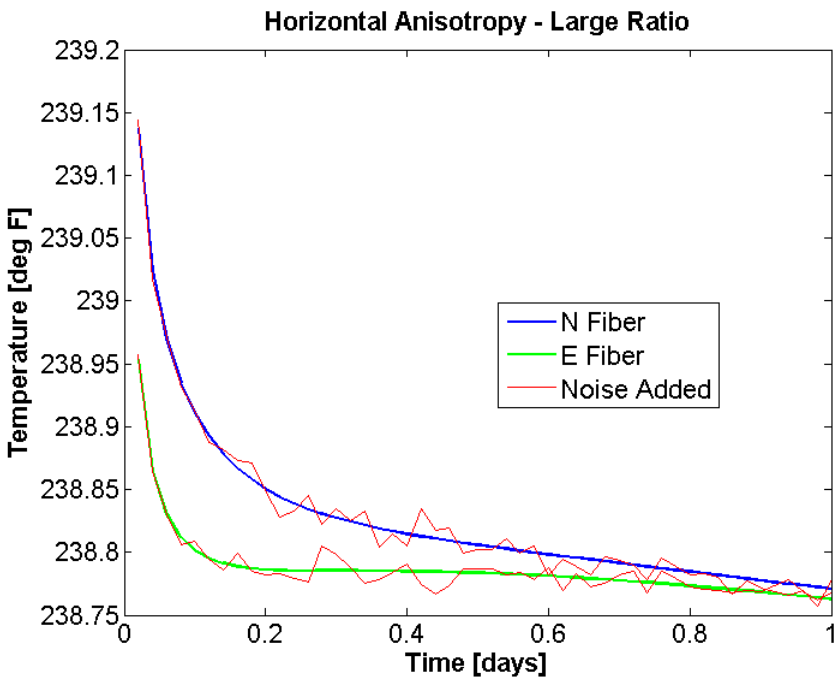

Figure 4.5: Temperature history with noise - small ratio

Although the relative error values were quite small and demonstrate the ability of the nonlinear regression algorithm to converge to the correct solution, the introduction of error with the addition of noise can be explained by examining the temperature history plots. When comparing the two extremes, the small and large ratio scenarios, the clear difference is the "distance" between the two plots of the North and East fiber measurements. This distance translates to the size of temperature difference between the fiber measurements and is reflective of the magnitude of the anisotropy ratio. Thus, the small ratio has a relatively smaller difference between the flow in orthogonal directions as compared to the large ratio, and thus has a relatively smaller difference in temperature measurements. With the addition of noise, the signals become convoluted and, particularly in the small ratio scenario, the measurements for each fiber sometimes overlap the trend for the other fiber. This behavior may

Table 4.3: Horizontal Anisotropy Regression Results - Noise Added

	Small		**Moderate**		**Large**	
	k_x (md)	k_y (md)	k_x (md)	k_y (md)	k_x (md)	k_y (md)
True Value	50	25	50	10	100	10
Initial Guess	20	20	20	20	20	20
Results	48.0	26.0	51.0	9.82	100.8	9.91
Relative Error	4.0%	4.0%	1.9%	1.8%	0.8%	0.9%

cause the parameter estimation procedure to have difficulty in converging to the exact solution (although no such difficulty was found in the scenarios shown here).

4.2.2 Discussion of Temperature Behavior

The temperature behavior that is associated with horizontal permeability anisotropy is discussed next. In comparison with the vertical anisotropy case, where the temperature signals represented the discrepancy between vertical and horizontal flow, the temperature behavior for the horizontal case should be expected to demonstrate the discrepancy between flow in the two horizontal, orthogonal directions. Because no vertical flow was considered for the horizontal anisotropy case, the spatial temperature distribution in the horizontal plane only will be examined for discussion. In addition, the temporal distributions of the temperature signals at the locations of the blocks representing DTS fibers will be included for further discussion.

The spatial distribution of the temperature signal clearly shows distinct, anisotropic behavior in the near-wellbore region. Several figures of this distribution were produced for better visualization of the effect of anisotropic permeability and flow on the reservoir temperature. Note that these figures were taken from the results of the large ratio scenario, in order to better demonstrate the effects of anisotropy. Figure 4.6 first shows the birds-eye view of the reservoir in its entirety at the initial time

step of the simulation. This graphic shows that the temperature distribution has an elliptical shape to it, with the extent of the larger changes from the initial temperature ($T_0 = 240$ °F) occurring in the direction with greater directional permeability ($k_x = 100$ md).

Figure 4.7 and Figure 4.8 show the temperature distribution in the near-wellbore region, at a zoomed in perspective from Figure 4.6. These two figures also show the progression in time over the duration of the test, first at the initial timestep, then at the final timestep occurring at one day. The progression once again shows the elliptical nature of the distribution at early time, but also shows that this behavior continues through the end of the test. These figures also give a visualization of the temperature difference between fibers at the orthogonal blocks neighboring the wellbore. Due to the elliptical nature, the temperature of the fiber coinciding with the greater directional permeability experiences a greater change in temperature with time. Of course, the magnitude of the temperature distribution as a whole changes with time as well, with each block having a decreasing trend. This trend was seen previously in the temperature history plots including the noisy signal (see Figure 4.3) and will be touched on later in the section as well.

The temporal history of the temperature measurements for each scenario enhances the understanding of the relationship between temperature behavior and horizontal anisotropy. Figure 4.9, Figure 4.10, and Figure 4.11 show the temperature history plots for the small ratio scenario, moderate ratio scenario, and large ratio scenario, respectively. Each plot also contains the temperature history attributed to the isotropic initial guess given to the nonlinear regression algorithm, where it was assumed initially that $k_x = k_y$ (see Table 4.1).

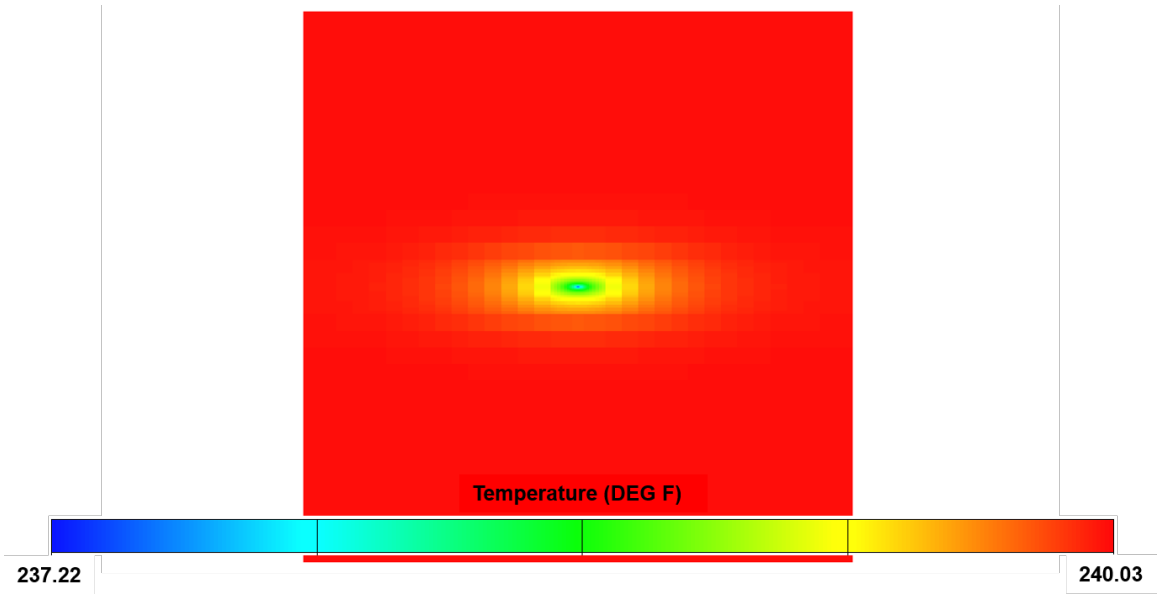

Figure 4.6: Spatial distribution of temperature - whole reservoir (1665 ft. $\times$ 1665 ft.)

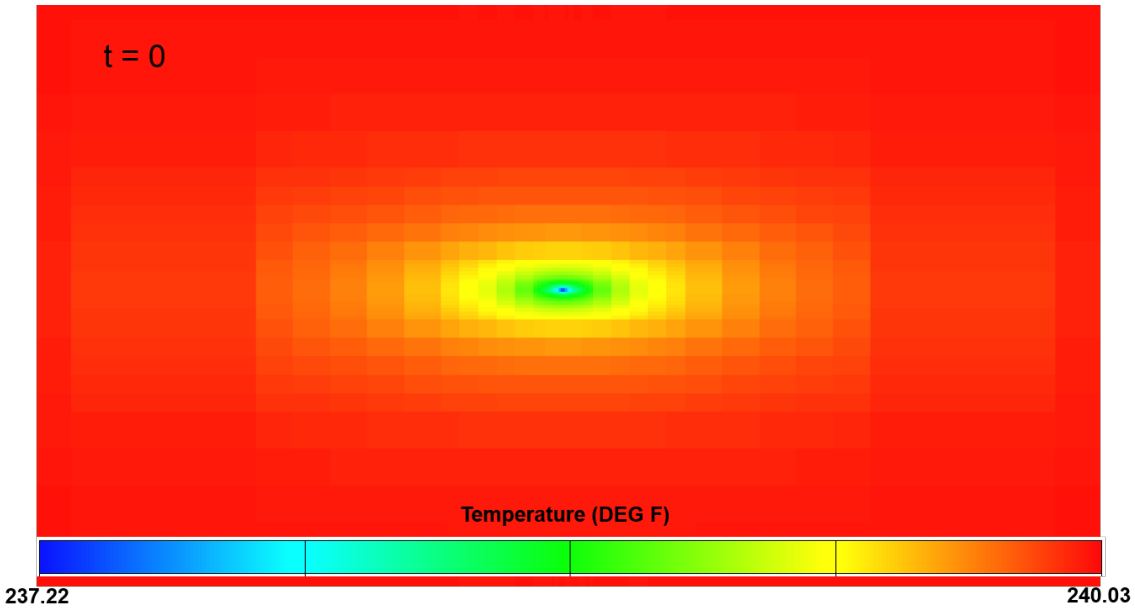

Figure 4.7: Spatial distribution of temperature at early time - zoomed in to near-wellbore region (300 ft. $\times$ 150 ft.)

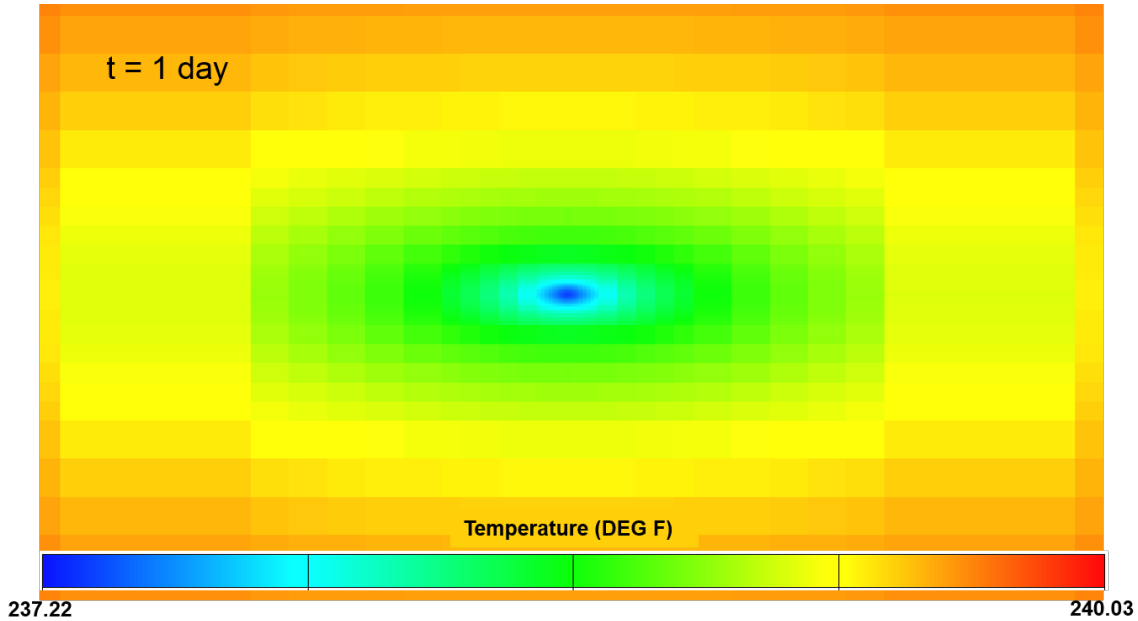

Figure 4.8: Spatial distribution of temperature at end of test - zoomed in to near-wellbore region (300 ft. × 150 ft.)

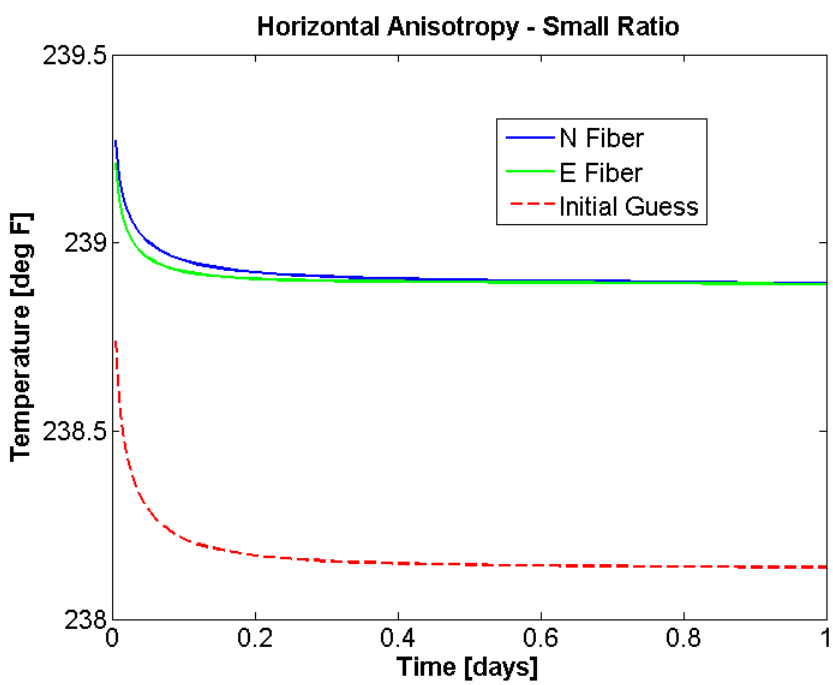

Figure 4.9: Temperature history - small ratio

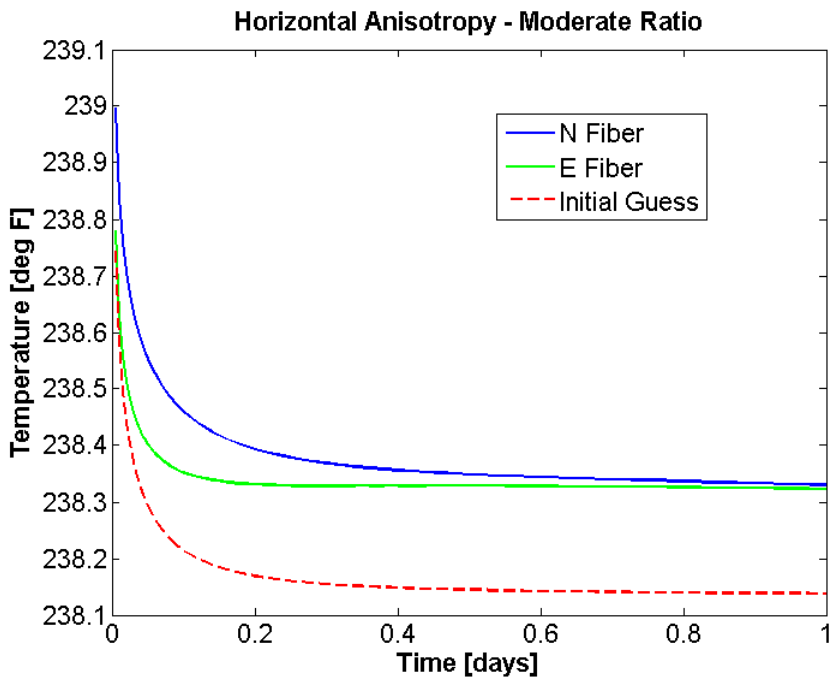

Figure 4.10: Temperature history - moderate ratio

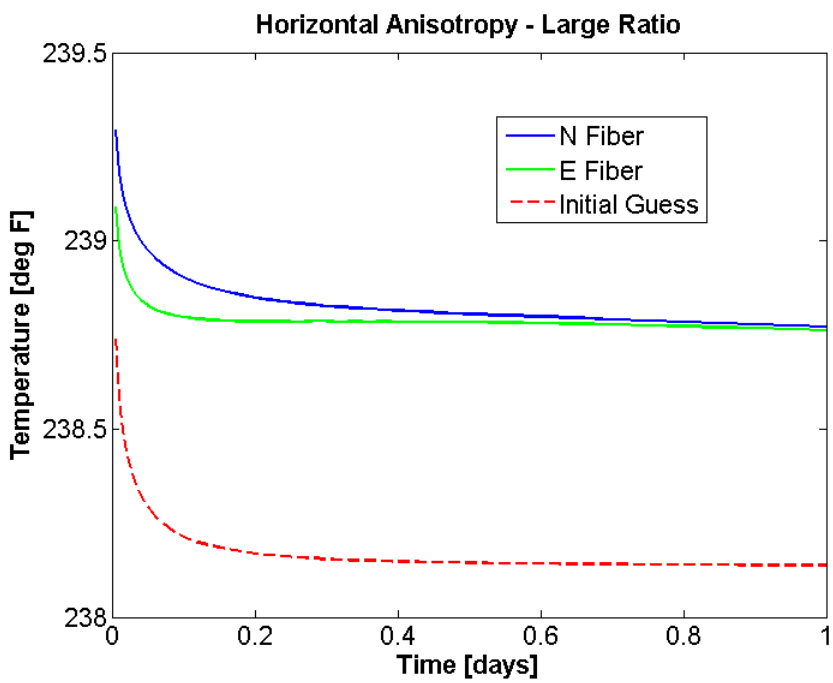

Figure 4.11: Temperature history - large ratio

The most prominent feature of the temperature history plots is the difference between the measurements taken at the North and East fibers. The magnitude of this difference was reflective of the magnitude of the anisotropy ratio that was investigated. Thus it is expected that the small ratio would result in a small difference between the measurements, and vice versa. The existence of such a difference in measurements was itself representative of the effects of anisotropy; larger values of permeability in a certain direction lead to greater flow in that direction, and temperature signatures that reflect this behavior.

Another relevant result from the analysis of horizontal anisotropy was that the temperature difference noted above proved to be a significant factor in the successful estimation of the directional permeability values. Each of the temperature history plots show a difference between the fiber measurements for the duration of the test, however at late time, the signals tend towards each other such that the temperature difference tends toward zero. Figure 4.12 shows a plot of this difference for the duration of the test, where the trend towards zero is more noticeable. In all the regression analyses completed for this horizontal anisotropy case, the existence of this temperature difference was significant in converging to the correct solution. Importantly, the use of the portion of the transient data where the temperature difference is greatest was a significant factor in the parameter estimation. By comparison, Figure 4.13 shows a plot of the temperature difference for the same test as Figure 4.12, but extended to include an additional day of temperature data. The plot clearly shows that the early transient part has a more prominent temperature difference, and was thus the preferred data to use in the parameter estimation procedure. Data after 1 day would not be as effective.

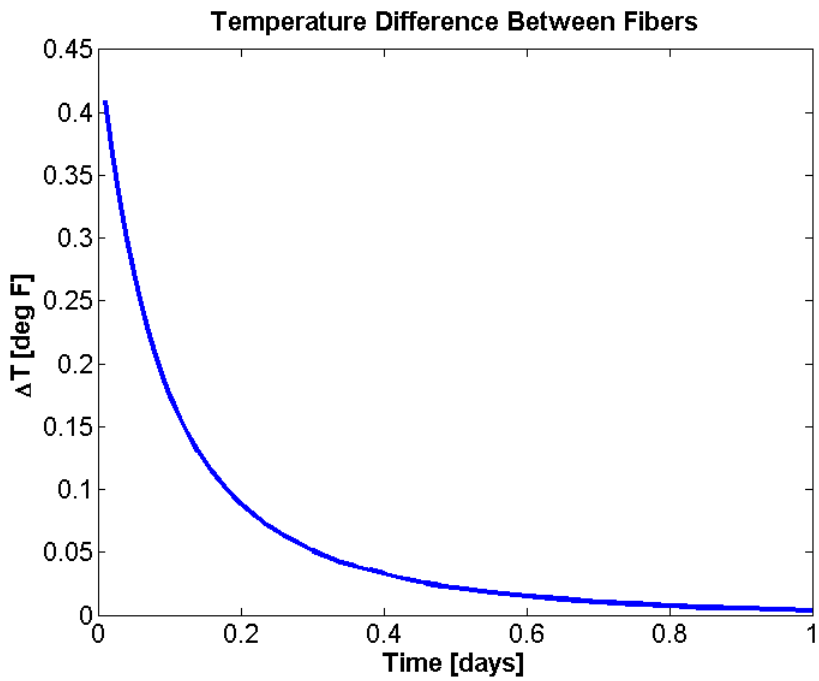

Figure 4.12: Temperature difference between fibers - normal one day test length

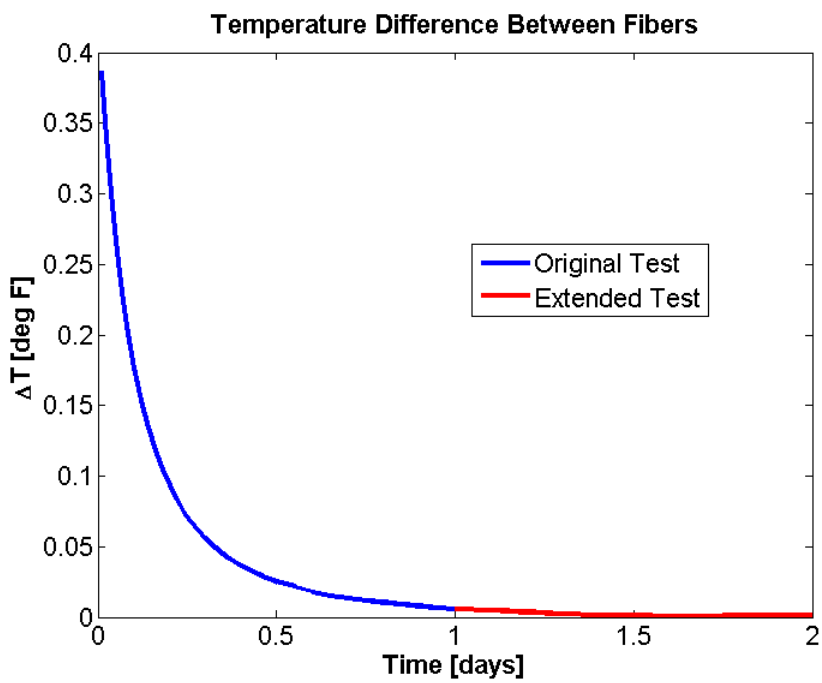

Figure 4.13: Temperature difference between fibers - test extended to two days length

Finally, we note that much of the analysis for the horizontal anisotropy case was completed with no regard to any other data but the temperature measurements. However, in the context of a traditional well test, the pressure data would provide additional information about the reservoir properties as well. To that end, the diagnostic pressure plot for the moderate ratio scenario is shown in Figure 4.14. Also included in the figure is the temperature difference plot for the same scenario, with a test length of two days. One interesting result comes from noting the time at which pseudosteady state behavior (unit slope on derivative plot) begins, in this case at approximately 24 hours. The temperature difference plot shows that, at about the same point in the test, the difference between the temperature measurements becomes very small. The fact that these phenomena are related demonstrates the coupled behavior of the temperature and pressure transients. It is possible that, at the point that the boundaries of the reservoir are felt by the pressure signal (i.e. the onset of pseudosteady state), the temperature signals measured by the fibers begin to "see" fluid with temperatures that reflect the far-field values (e.g. initial reservoir temperature). Thus, as the flow in orthogonal directions progresses through time, the far-field effects may become more prominent, and this behavior coincides with pseudosteady state behavior measured with the pressure signal.

4.3 Anisotropy in Skin

With the existence of horizontal permeability anisotropy, it would be expected that anisotropy in the skin effect, or near-wellbore damaged zone, would exist as well. As many sources describe (see Horne[6]), the skin effect is manifested as a zone of reduced permeability, lower than that of the reservoir at large. However, traditional well test analysis considers skin as a *circular* damaged zone that can be described by the reduced permeablity value and the radius of the circular zone. In the scenario

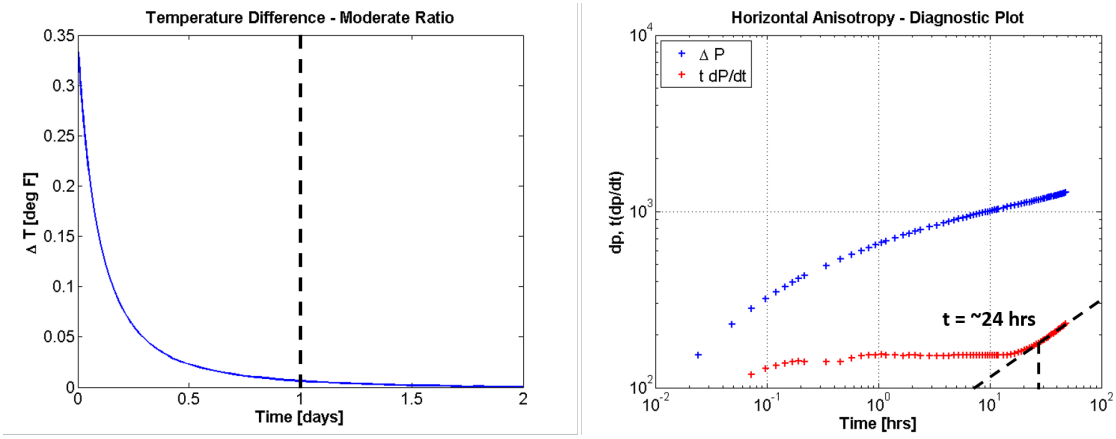

Figure 4.14: Temperature difference plot (left) and associated diagnostic plot (right)

where horizontal anisotropy is inherent in the subsurface, this damaged zone can no longer be assumed to have a circular shape. Instead, the zone will take a shape that reflects the magnitude of distinct directional permeability values. For this investigation, an *elliptical* damaged zone was used to model the skin surrounding the well.

Of particular note in this analysis is the choice of dimensions of the ellipse that constitutes the damaged zone. While previous studies may describe such an ellipse using an additional skin factor (see Stanislav, Easwaran, and Kokal[12]), the dimensions of the zone are undetermined. For this study on anisotropy in skin, it was assumed that the ratio of the major axes of the ellipse matches the anisotropy ratio of directional permeability values. Figure 4.15 includes two visualizations of a scenario where anisotropy in skin exists. In the gridded figure, the major axes lengths are described by "a" and "b", and the ratio of these lengths were assumed to match the anisotropy ratio (e.g. $a/b = k_x/k_y$). Additionally, much like the isotropic case, the damaged zone in the anisotropic case is characterized by reduced permeability values. However, for the horizontal anisotropy study, the reduced values are applied in both directions, and the fraction of the full-field values are kept consistent in each direction

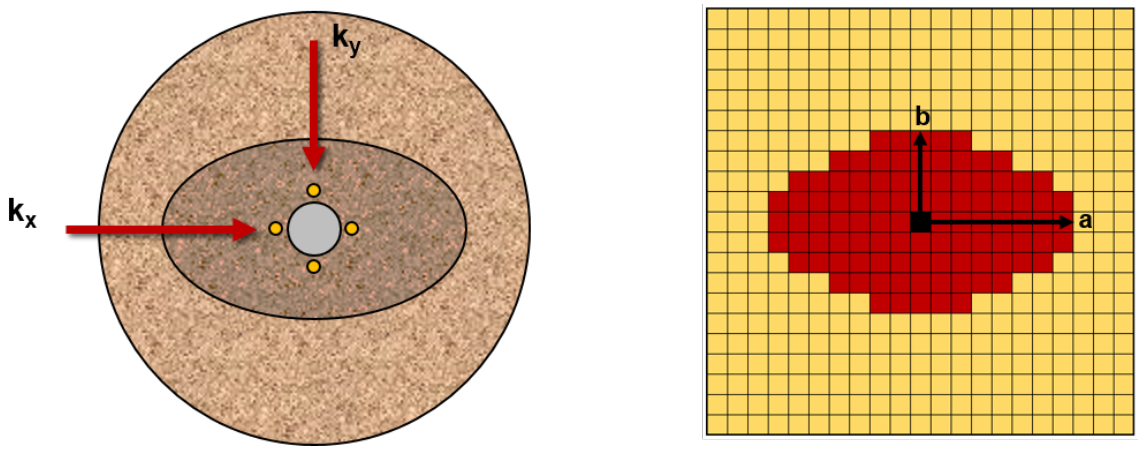

Figure 4.15: Graphics showing scenario with anisotropy in skin

Table 4.4: Summary of Anisotropic Skin Scenario

	Horizontal Anisotropy with Skin			
	k_x (md)	k_y (md)	k_{dx} (md)	k_{dy} (md)
True Value	150	50	30	10
Initial Guess	100	100	20	20

(e.g. $k_{dx} = 0.2 \times k_x$, $k_{dy} = 0.2 \times k_y$).

The scenario including anisotropy in skin was modeled in Eclipse by gridding an elliptical zone with the ratio of the major axes equal to the permeability anisotropy ratio. This translated to the ratio of the number of grid blocks in each direction being equal to the anisotropy ratio. Figure 4.16 gives a visualization of such a configuration when applied to the Cartesian grid in Eclipse. Apart from this change, all other simulator parameters remained the same as those used in the regular permeability anisotropy case. Finally, Table 4.4 includes the details for the only scenario investigated and applied to the parameter estimation procedure. Note that the field directional permeability values are denoted by k_x and k_y, and the damaged zone values are denoted by k_{dx} and k_{dy}.

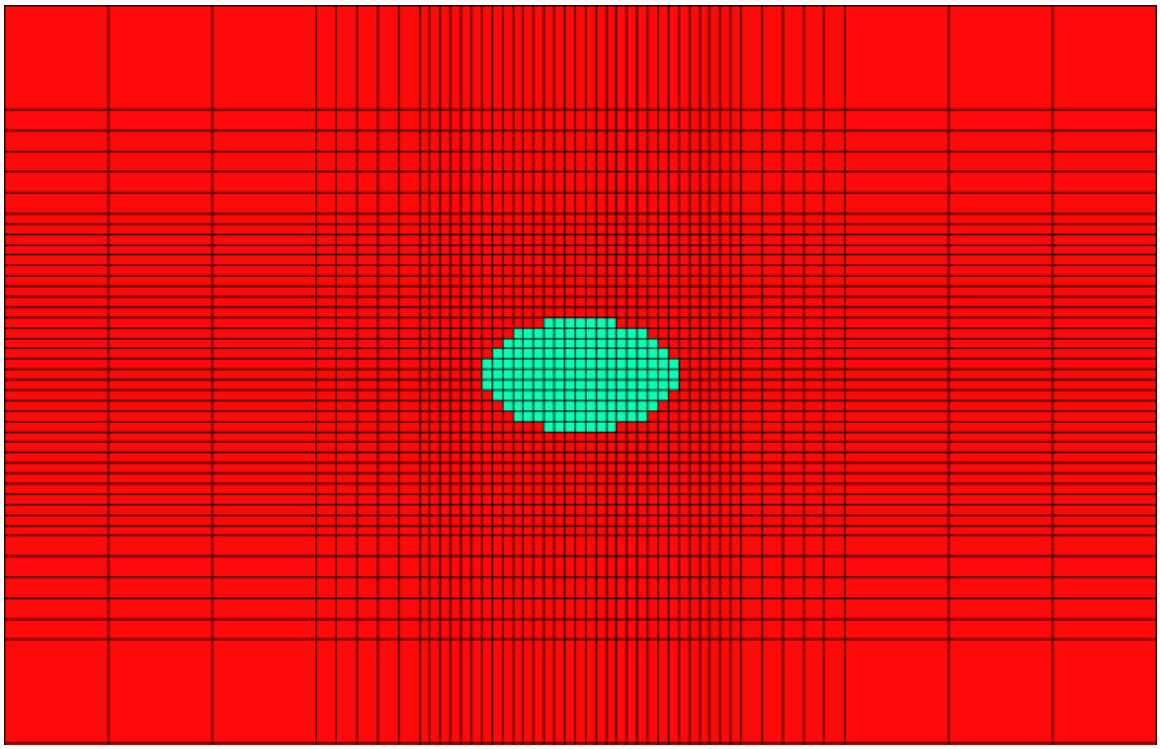

Figure 4.16: Elliptical damaged zone applied to simulation grid

4.3.1 Results and Discussion

The results of the parameter estimation procedure applied to the anisotropic skin case proved to be very accurate in determining the damaged zone properties (k_{dx} and k_{dy}), but was less accurate in estimating the field permeability values (k_x and k_y). Table 4.5 includes a summary of the scenario investigated and the regression results. The relative error is again described by Equation 4.1. While the algorithm converged to the correct solution for the damaged zone properties, a small amount of error ($< 5\%$) was present in the results for the field permeability values.

A small discussion of the temperature behavior in the anisotropic skin scenario follows. First, the pressure field at early time is shown in Figure 4.17, which gives a visualization of the pressure values in the near-wellbore region. The additional pressure drop that is characteristic of the skin effect can clearly be seen in this region, demonstrating the approximate shape of the elliptical damaged zone. While this graphic is meant to orient the reader in the properties of the damaged zone, the spatial distribution of the temperature measurements gives more insight into the relationship between anisotropy in skin and temperature transient behavior. Figure 4.18, Figure 4.19, and Figure 4.20 each show the spatial distribution of temperature at different points in the one-day test; at the initial timestep, at 0.25 days, and at the final timestep, respectively.

Of particular note in the progression of the temperature field with time is the distinct temperature behavior in the two separate regions of the reservoir, the damaged zone and the unaltered zone. In the unaltered reservoir, outside the zone of reduced permeability, the temperature signal behaves similarly to the anisotropic permeability case, following a decreasing trend with time. The distribution, in combination with the

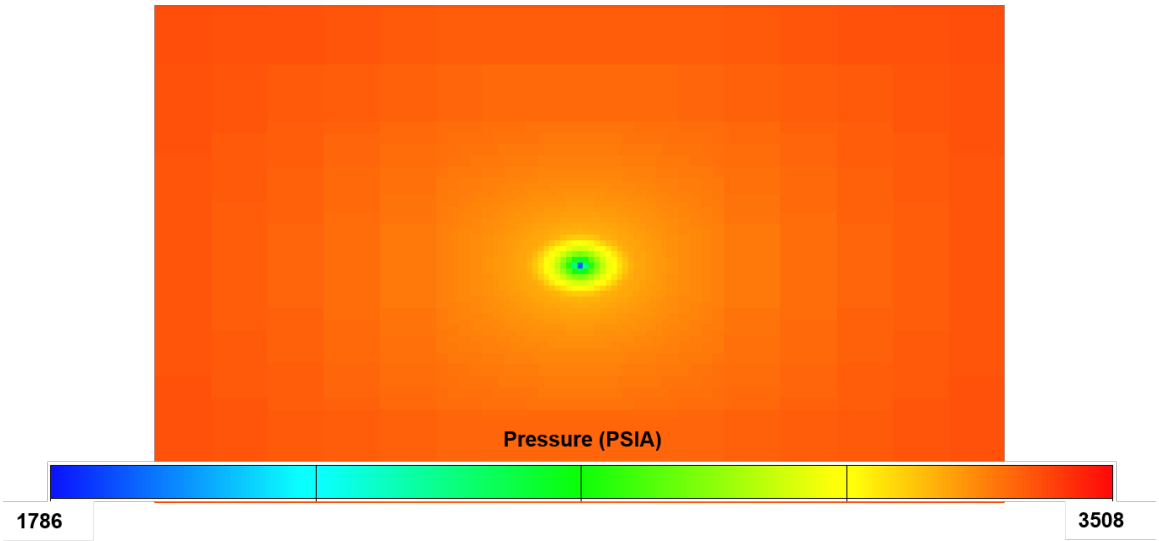

Figure 4.17: Pressure field at early time - anisotropic skin scenario

colorbar, shows that the extents of the figures move from orange-colored to yellow-colored, denoting a slight decrease in temperature for the duration of the test. In the near-wellbore, damaged zone region however, the temperature actually increases with time. Once again using the colorbar as a reference, the temperature measurements in the near-wellbore region progresses from blue-colored to green-colored, denoting a slight *increase* in temperature and a departure from the behavior seen in previous anisotropic cases involving no skin effect. The temperature history plots shown in Figure 4.21 and Figure 4.22 show these trends more clearly. Note that the measurements in Figure 4.22 are block temperature (BTEMP) measurements at the grid blocks in the x- and y-directions just outside of the zone of reduced permeability. Thus, they have the full-field, unaltered directional permeability values.

A possible explanation for the reversal of temperature behavior in the damaged zone region comes from the obvious distinction between the permeability values in the two regions. Fluid coming from the unaltered reservoir encounters the zone of reduced

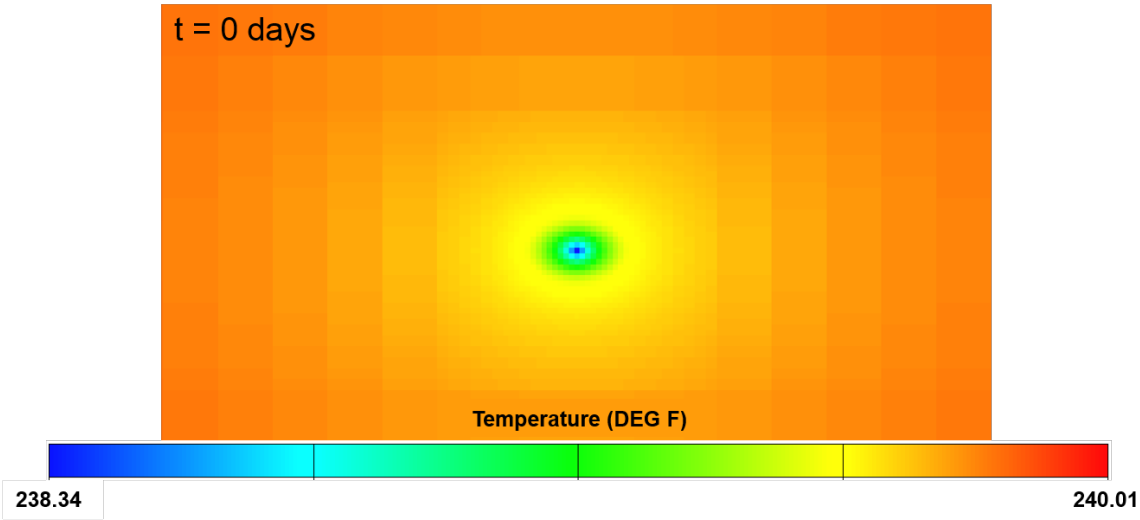

Figure 4.18: Temperature distribution at initial timestep - anisotropic skin scenario

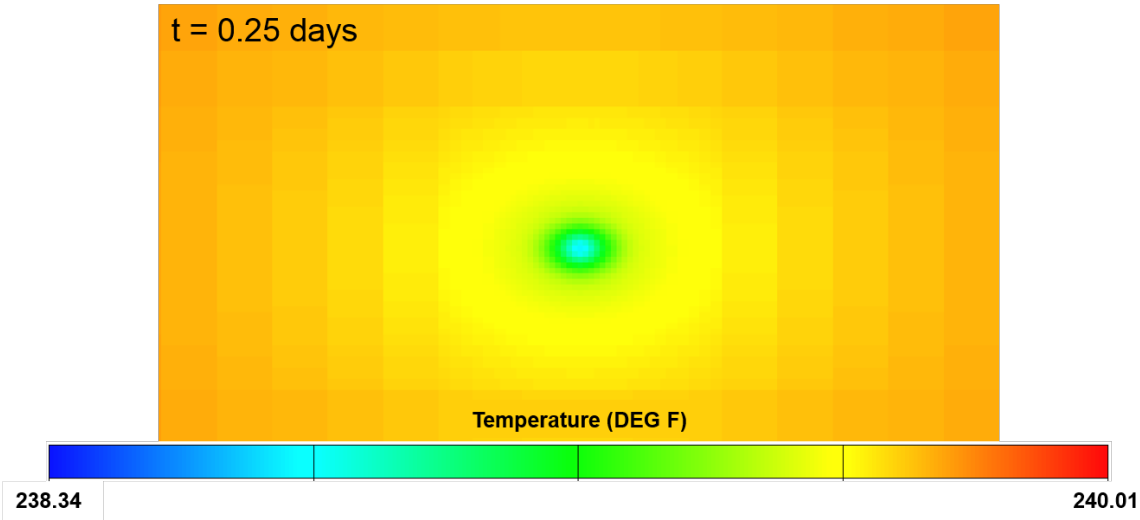

Figure 4.19: Temperature distribution at early time - anisotropic skin scenario

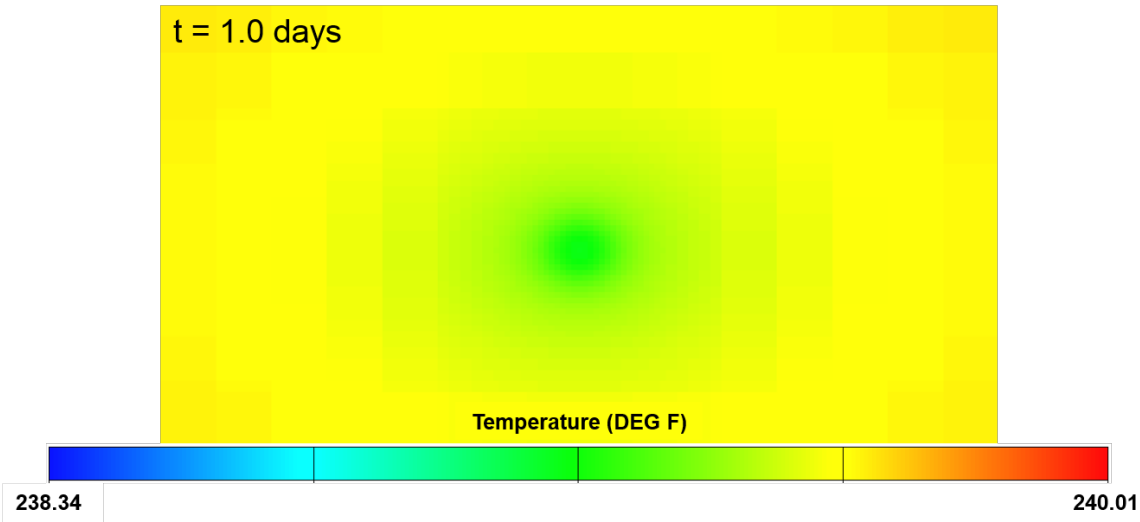

Figure 4.20: Temperature distribution at final timestep - anisotropic skin scenario

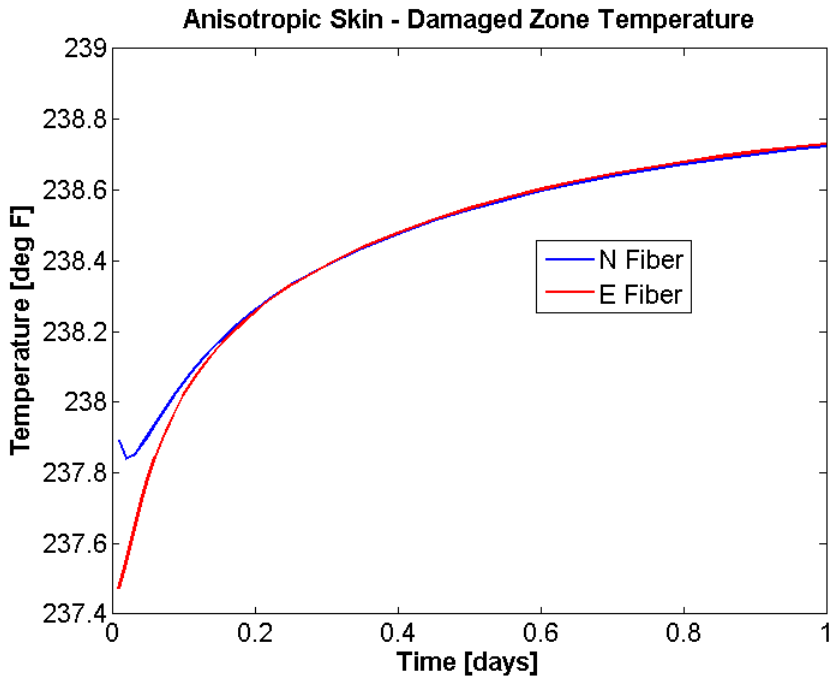

Figure 4.21: Temperature history of fiber measurements **inside** the damaged zone region

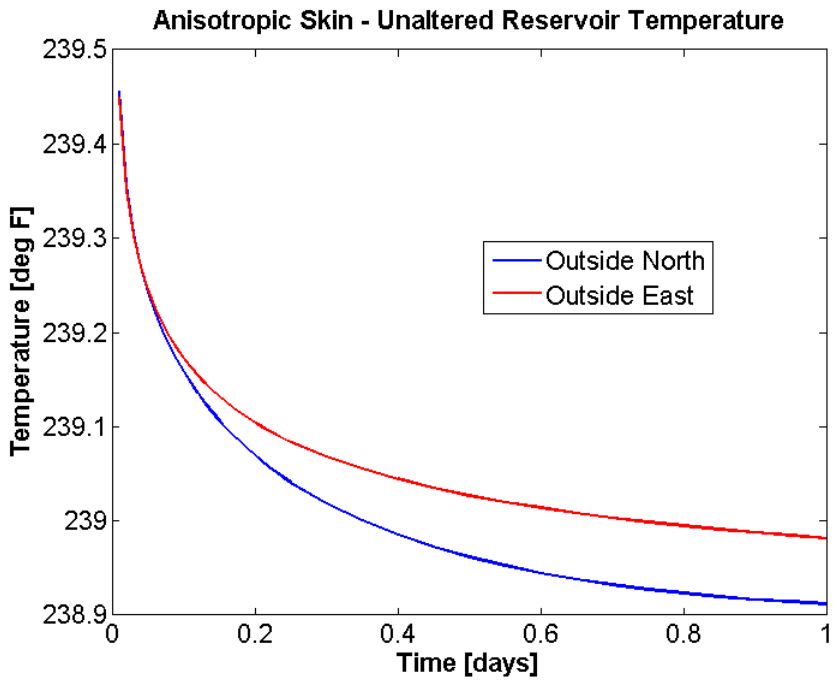

Figure 4.22: Temperature history of blocks **outside** the damaged zone

permeability, causing an increase in pressure drop. This increase in pressure drop would be the cause of the heating effect due to Joule-Thomson behavior of the liquid.

Table 4.5: Anisotropic Skin Regression Results

	Horizontal Anisotropy with Skin			
	k_x (md)	k_y (md)	k_{dx} (md)	k_{dy} (md)
True Value	150	50	30	10
Initial Guess	100	100	20	20
Results	157.3	47.7	30.0	10.0
Relative Error	4.9%	4.6%	0%	0%

4.4 Summary

The results and discussion of the temperature behavior associated with horizontal anisotropy in permeability and skin were presented in this chapter. The combination of a novel multiple DTS completion and the temperature measurements at specific fiber locations led to the main results of this study of horizontal anisotropy. This study was also extended to investigate the effects of anisotropic skin on temperature behavior, which included a regression analysis for estimating both the field and damaged zone directional permeability values as well.

The study of the horizontal anisotropy case proved to be very successful and, along with the results from the vertical case, further confirmed the potential usage of temperature transient analysis for parameter estimation purposes. This chapter showed that in three distinct scenarios of horizontal permeability anisotropy, represented by small, moderate, and large anisotropy ratios (k_x/k_y), the nonlinear regression algorithm was very accurate in estimating the directional permeability values. The addition of synthetic noise to the temperature data, an attempt to replicate real DTS data, also proved to be successful when applied to the parameter estimation procedure. The extension of the analysis to include anisotropic skin, modeled as an elliptical zone of reduced permeability with anisotropy ratio consistent with the full field values, also had success in estimating the directional permeability values. The nonlinear regression algorithm was able to estimate both the field permeability values as well as the damaged zone values in the horizontal directions with a high degree of accuracy. Finally, the temperature behavior in both the spatial and temporal domains were discussed for each anisotropy scenario. From this, the resulting temperature signatures gave better insight into the underlying temperature transient behavior when anisotropy in permeability and/or skin exists.

Chapter 5

Conclusion and Future Work

5.1 Conclusions

As the use of temperature transient analysis in the determination of reservoir properties becomes more widespread, novel ways to interpret the temperature data are being researched. In this study, temperature measurements from a Distributed Temperature Survey (DTS) test allowed for an investigation into the relationship between temperature transient behavior and anisotropy in permeability and skin.

Two different types of anisotropy were analyzed in this report, vertical anisotropy and horizontal anisotropy. In the vertical case, permeability anisotropy in the vertical and horizontal directions was assumed, and in the horizontal case, permeability anisotropy in orthogonal, horizontal directions was assumed. In the horizontal case, the analysis was extended to include effects of anisotropy in skin.

In Chapter 3, the methodology behind the study was discussed, based on the thermal simulations that were run for the purposes of the research. Two different types of grids were created for the two anisotropy cases investigated, a radial grid for the

vertical case and a Cartesian grid for the horizontal case. The thermal simulator used typical values for the fluid, rock, and thermal properties. Also in this chapter was the introduction of the parameter estimation procedure. A Matlab function was used for the nonlinear regression algorithm that updated the directional permeability values until convergence.

In Chapter 4, the vertical anisotropy case was detailed. Three scenarios were created that described the magnitude of the anisotropy ratio between the vertical and horizontal permeability values (k_v and k_h). Using the forward model temperature data and the data from an isotropic initial guess of permeability values, the nonlinear regression was applied to each scenario. In all three cases, the results of the algorithm were very accurate, correctly estimating the directional values with little to no error. In an attempt to replicate real DTS data, synthetic noise was included in the forward model signals for the three scenarios and put through the parameter estimation procedure. With the addition of noise, error was introduced to the results of the regression, and it was noted that the magnitude of temperature difference over the duration of the test could be the cause of the error. Finally, Chapter 4 also discussed the temperature behavior associated with vertical anisotropy, and noted the discrepancies between the anistropic flow that led to the distinct temperature signals.

In Chapter 5, the horizontal anistropy case was described. The horizontal case coupled the use of temperature transient analysis with a unique type of DTS completion with multiple fibers (two in this case) distributed around the circumference of the casing. The same type of analysis as in the vertical case was completed in the horizontal case, where three anisotropy scenarios were created for use in the parameter estimation procedure. The regression was successful in estimating the directional permeability values (k_x and k_y) in all three scenarios. Even with the addition of noise,

the regression algorithm was still able to find the correct solution with minimal error. Chapter 5 also discussed the relationship between horizontal anisotropy and the observed temperature behavior. Both the spatial and temporal distributions of the temperature measurements gave more insight into the relationship, by noting factors such as the existence of a nonzero temperature difference between fibers being indicative of anisotropic flow and useful in the regression analysis. This model was also extended to include anisotropy in skin, where it was noted that inherent anisotropy in the reservoir would result in anisotropy in the zone of reduced permeability as well. The parameter estimation procedure applied to this scenario was successful in estimating the near-wellbore, damaged zone properties (k_{dx} and k_{dy}), but a small amount of error resulted from the estimation of the full-field, unaltered properties (k_x and k_y). The temperature behavior of the anisotropic skin scenario was also discussed in this chapter.

5.2 Future Work

Some possible directions for future research include:

5.2.1 Confirmation of Results

The studies presented here used the Eclipse 300 thermal simulator for the generation of temperature data. This included the generation of temperature data for the forward model used in the regression analysis. Although the type of DTS completion necessary for such an investigation is unique, real temperature data resulting from such a configuration would allow for a confirmation of the results reported here. In the absence of real data, the setup of a separate thermal simulator would also provide confirmation of the ability of the method.

5.2.2 Model Extension

The novelty of the analysis required that many of the model parameters remain simple. For example, the two more prevalent simplifications in this research were the use of a vertical well and the assumption of single-phase oil flow only. Extensions to this model, such as a horizontal or deviated well or the inclusion of multiphase flow would provide more comprehensive results.

5.2.3 Further Investigation of Anisotropic Skin Effects

The literature review completed for this study provided little information on the existence of anisotropy in skin, and less about the relationship between such a phenomena and its effect on temperature behavior. The procedure that was followed in analyzing the relationship (see Section 4.3) was based on several assumptions. Further research into the properties of such a scenario would allow for a better understanding of the model that includes both anisotropy in permeability and skin.

Nomenclature

k_h	Horizontal permeability (md)
k_v	Vertical permeability (md)
k_x	Permeability in x-direction (md)
k_y	Permeability in y-direction (md)
k_{dx}	Reduced permeability in x-direction (md)
k_{dy}	Reduced permeability in y-direction (md)
P	Pressure (psi)
S_o	Oil saturation
T	Temperature (°F)
t	Time (days)
T_0	Initial reservoir temperature (°F)

References

[1] Ayan et al., 1994. Measuring permeability anisotropy: The latest approach. Oilfield Review, Vol. 6, No. 4, pgs. 24–35.

[2] Batocchio, Marcelo AP et al. 2010. Case History-Steam Injection Monitoring with Optical Fiber Distributed Temperature Sensing. SPE Intelligent Energy Conference and Exhibition, Society of Petroleum Engineers.

[3] Brown, G., Field, D. Davies, J., Collins, P. and Garayeva, N. 2005. Production Monitoring Through Openhole Gravel-Pack Completions Using Permanently Installed Fiber-Optic Distributed Temperature Systems in the BP-Operated Azeri Field in Azerbaijan. SPE 95419 presented at the SPE Annual Technical Conference and Exhibition, Dallas, TX, USA.

[4] Ehlig-Economides, C and Ebbs, D and Meehan, DN. 1990. Factoring anisotropy into well design. Oilfield Review, Vol. 2, No. 4, pgs. 24–33.

[5] Furniss, J.P., Schouten, J., Bottomley, W., and Taylor, H. 2014. Reservoir Characterisation Using Distributed Temperature Sensing in CSG Development: Application in the Surat Basin Queensland Australia. SPE Asia Pacific Oil & Gas Conference and Exhibition, Society of Petroleum Engineers.

[6] Horne, R. 1995. "Modern Well Test Analysis", Petroway, Inc., California, 2nd edition.

[7] Koelman, JMVA, Lopez, JL, and Potters, JHHM. 2012. Fiber optic technology for reservoir surveillance. IPTC 14629 presented at the International Petroleum Technology Conference, Bangkok, Thailand.

[8] Mabunda, H. 2014. Utilization of Temperature Data to Determine Reservoir Thickness. Stanford University Masters report.

[9] Matlab. 2013. version 8.2.0.348 (R2013b), The MathWorks Inc., Massachusetts.

[10] Ouyang, L. and Belanger, D. 2006. Flow Profiling by Distributed Temperature Sensor (DTS) System Expectation and Reality. SPE Production and Operation Journal, SPE 90541.

[11] Ramey Jr, HJ. 1975. Interference analysis for anisotropic formations-a case history. J. Pet. Tech, Vol. 27, No. 10, pgs. 1290–1298.

[12] Stanislav, JF and Easwaran, CV and Kokal, SL. 1992. Elliptical flow in composite reservoirs Journal of Canadian Petroleum Technology, Vol. 31, No. 10, pgs. 47–50.

[13] Sui, W, Zhu, D, Hill, A.D. and Ehlig-Economides, C.A. 2008. Determining Multilayer Formation Properties From Transient Temperature and Pressure Measurements. SPE 116270 presented at the SPE Annual Technical Conference and Exhibition, 21-24 September 2008, Denver, USA.

[14] Sui, W, Zhu, D, Hill, A.D. and Ehlig-Economides, C.A. 2008. Model for Transient Temperature and Pressure Behavior in Commingled Vertical Wells. SPE 115200-MS presented at the SPE Russian Oil and Gas Technical Conference and Exhibition, 28-30 October 2008, Moscow, Russia.

[15] Wang, Z. 2012. The Uses of Distributed Temperature Survey (DTS) Data. Stanford University PhD dissertation.

Appendix A

Sample Input File

```
RUNSPEC          ==================

TITLE
 Horizontal Anisotropy/

START
1 'JAN' 2015/

FIELD

OIL
WATER
DEADOIL

THERMAL

DIMENS
---Nx   Ny   Nz
    71   71   20 /

WELLDIMS
 1 /

COMPS
 1 /

PARALLEL
 3 /


GRID                    ========================

INIT
GRIDFILE
 2 /

TOPS
```

```
5041*5000
/

INCLUDE
     'gridX.dat'
/
INCLUDE
     'gridY.dat'
/

DZ
15123*20
70574*10
15123*20
/

EQUALS

          'PORO'          0.001    1   71   1   71   1    3    /
          'PORO'          0.230    1   71   1   71   4    17   /
          'PORO'          0.001    1   71   1   71   18   20   /

/

THCROCK
100820*36/

THCOIL
100820*36/

THCWATER
100820*36/

HEATCR
100820*35
/

INCLUDE
  'permX.dat'
/
INCLUDE
  'permY.dat'
/
INCLUDE
  'permZ.dat'
/


PROPS                    ==============================

VISCREF
2750/

PVTW
-- Pref | wat FVF @Pref | wat compres | visco@Pref | viscosibility @Pref
   14.7        1.0            5.0E-7            1.0              0.0 /

--  PRESSURE    RS        BO       VISO       CO       VISOSIBILITY
--   [psia] [mscf/stb] [rb/stb]   [cp]    [1/psia]     [1/psia]
PVCO
```

```
  14      0     1      .6     1.E-05        0.0
  2750    0          .8     .6     1.E-05        0.0
/

ZI
 1.0
/

OILCOMPR
5E-7     0.000178          0/

OILSPECH
0.15/

ROCK        -- reference Pressure and rock compressibility
         14.7     1E-6
/

DENSITY   -- oil wat gas @surface(lbm/scf)
         40.0  62.238 0.0702
/

OILVISCT
         75       10.583
        100       9.061
        150       6.775
        200       5.183
        250       4.0434
        300       3.2082
        350       2.5833
        500       1.4498
        800       1.4498
/


-- SWAT    KRW    PCOW
SWFN

--    Sw          Krw              Pcow
   ------       -------            ----
     0.27         0.0                24
     0.4397       0.0476              6
     0.51         0.0952              3
     0.56         0.1428              2
     0.62         0.1905            1.5
     0.65         0.2381            1.2
     0.68         0.2857            0.0
     0.7151       0.3333            0.0
     1            0.50              0.0//
-- FOR OIL-WATER AND OIL-GAS-CONNATE WATER CASES
--
-- SOIL       KROW
SOF3

--    So    Krow       Krog
   ------  -------    -------
     0.27      0         0
     0.4397    0.1       0.1
     0.51      0.2857    0.2857
     0.56      0.3       0.3
     0.62      0.4       0.4
```

```
    0.65      0.6      0.6
    0.68      0.8      0.8
    0.7151    0.99     0.99
    1         1        1   /

SGFN
    0.0     0.0        0.0
    0.04    0.0        0.2
    0.1     0.022      0.5
    0.2     0.1        1.0
    0.6     0.5        3.0
    0.88    1.0        3.9
/


SOLUTION   == initial state of solution variables ==================

RTEMPVD
5000 240
6000 255
/

EQUALS
        'SOIL'      1       1  71  1  71  1  20  /
        'SWAT'      0       1  71  1  71  1  20  /
        'PRESSURE'  3500    1  71  1  71  1  20  /
        'TEMPI'     240     1  71  1  71  1  20  /
/


SUMMARY    == output written to summary *.RSM file ================
RUNSUM     -- additional table in *.PRT file
WOPR
 'PROD'

WWPR
 'PROD'


WBHP
  'PROD'

FPR        -- Average reservoir pressure
FOPT       -- Cumulative oil production of the field
FWPT       -- Cumulative water production of the field
FOE        -- request oil recovery


--WTEMP        ---WELL TEMPERATURE
--'PROD'

BTEMP

36 35 11    -- 0.5 ft. from well in +y direction
37 36 11    -- 0.5 ft. from well in +x direction

/


SCHEDULE   == operations to be simulated ==========================
```

```
RPTSCHED
TEMP /

RPTRST     -- request restart file
BASIC=2 TEMP
/

WELSPECS    == WELL SPECIFICATION DATA ==================================
--    WELL    GROUP LOCATION   BHP     PI
--    NAME    NAME      I      J      DEPTH DEFN
      'PROD'  'W1'      36    36      -1  'OIL'    2*  'STOP'  /
/
COMPDAT     -- COMPLETION SPECIFICATION DATA
--    WELL   LOCATION              OPEN/ SAT CONN   WELL   KH   S   D   AXIS
--    NAME     I      J     K1   K2    SHUT   TAB FACT   DIAM
      'PROD'    36    36    4    17     'OPEN'   0     1*     0.3  /
/
WCONPROD    -- PRODUCTION WELL CONTROLS
--    WELL     OPEN/   CTRL       OIL   WATER    GAS   LIQU    RES    BHP
--    NAME     SHUT    MODE      RATE    RATE   RATE   RATE   RATE
      'PROD'   'OPEN'  'ORAT'    1000    4*                            50   /
/


NSTACK
50 /

TUNING
0.01  0.01  0.01  /
5*  /
2*  300  /

TSTEP
0.4
/

TUNING
0.05  0.05  0.05  /
5*  /
2*  300  /

TSTEP
0.6
/


END        ==================================================================
```